NeuroImage 262 (2022) 119551

Contents lists available at ScienceDirect

NeuroImage

journal homepage: www.elsevier.com/locate/neuroimage

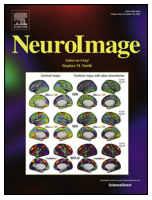

Structural connectivity of the ANT region based on human ex-vivo and HCP data. Relevance for DBS in ANT for epilepsy

Milan Majtanik[a,b], Frans Gielen[c], Volker Arnd Coenen[d,e], Kai Lehtimäki[f], Jürgen Konrad Mai[a,g,*]

[a] MRX-Brain GmbH, Moritz-Sommer-Str. 4., 40225 Duesseldorf, Germany
[b] Department of Informatics, Heinrich Heine University of Düsseldorf, Universitätsstraße 1, 40225 Düsseldorf, Germany
[c] Medtronic Bakken Research Center, Endepolsdomein 5, 6229 GW Maastricht, the Netherlands
[d] Department of Stereotactic and Functional Neurosurgery, Medical Center of University of Freiburg, Breisacher Straße 64, 79106 Freiburg im Breisgau, Germany
[e] Medical Faculty of the University of Freiburg, Breisacher Str. 153, 79110 Freiburg im Breisgau, Germany
[f] Department of Neurosciences and Rehabilitation Tays, PO Box 2000, FI-33521 Tampere University and Tampere University Hospital, Tampere, Finland
[g] Department of Neuroanatomy, Heinrich Heine University of Düsseldorf, Universitätsstraße 1, 40225 Düsseldorf, Germany

ABSTRACT

Objective: Deep Brain Stimulation (DBS) in the Anterior Nucleus of the Thalamus (ANT) has been shown to be a safe and efficacious treatment option for patients with Drug-Resitant focal Epilepsy (DRE). The ANT has been selected frequently in open and controlled studies for bilateral DBS. There is a substantial variability in ANT-DBS outcomes which is not fully understood. These outcomes might not be explained by the target location alone but potentially depend on the connectivity of the mere stimulation site with the epilepsy onset-associated brain regions. The likely sub-components of this anatomy are fiber pathways which penetrate or touch the ANT region and constitute a complex and dense fiber network which has not been described so far. A detailed characterization of this ANT associated fiber anatomy may therefore help to identify which areas are associated with positive or negative outcomes of ANT-DBS. Furthermore, prediction properties in individual ANT-DBS cases might be tested. In this work we aim to generate an anatomically detailed map of candidate fiber structures which might in the future lead to a holistic image of structural connectivity of the ANT region.

Methods: To resolve the various components of the complex fiber network connected to the ANT we used a synthetic pathway reconstruction method that combines anatomical fiber tracking with dMRI-based tractography and iteratively created an anatomical high-resolution fiber map representing the most important bundles related to the ANT.

Results: The anatomically detailed 3D representation of the fibers in the ANT region generated with the synthetic pathway reconstruction method incorporates multiple anatomically defined fiber bundles with their course, orientation, connectivity and relative strength. Distinctive positions within the ANT region have a different hierarchical profile with respect to the stimulation-activated fiber bundles. This detailed connectivity map, which is embedded into the topographic map of the MNI brain, provides novel opportunities to analyze the outcomes of the ANT-DBS studies.

Conclusion: Our synthetic reconstruction method provides the first anatomically realistic fiber pathway map in the human ANT region incorporating histological and structural MRI data. We propose that this complex ANT fiber network can be used for detailed analysis of the outcomes of DBS studies and potentially for visualization during the stimulation planning procedures. The connectivity map might also facilitate surgical planning and will help to simulate the complex ANT connectivity. Possible activation patterns that may be elicited by electrodes in different positions in the ANT region will help to understand clinically diverse outcomes based on this new dense fiber network map. As a consequence this work might in the future help to improve individual outcomes in ANT-DBS.

Abbreviations: 2t, optic tract; 2x, optic chiasm; ac, anterior commissure; Acc, accumbens nucleus; ACg, anterior cingulate cortex; AD, anterodorsal thalamic nucleus; AHB, Atlas of the Human Brain, 4th edition, 2015; al, ansa lenticularis; alic, anterior limb of internal capsule; AM, anteromedial thalamic nucleus; aMCG, anterior midcingulate gyrus; Amy, amygdala; ANT, anterior nucleus/nuclei of the thalamus; AS, area septi; athr, anterior thalamic radiation; AV, anteroventral thalamic nucleus; BNST, bed nucleus of the stria terminalis; Cd, caudate nucleus; CeM, central medial nucleus; CgG, cingulate gyrus; DB, diagonal nucleus of Broca; dMRI, diffusion-weighted Magnetic Resonance Imaging; DSf, dorsal superficial (laterodorsal) nucleus; DTI, Diffusion Tensor Imaging; ECx, entorhinal cortex; FA, fasciculosus nucleus; FMG, middle frontal gyyrus; fr, fasciculus retroflexus; fx, fornix; GPi, internal globus pallidus; Hb, habenula; Hip, hippocampus; ILF, intralaminar formation; Ilm, medial intralaminar formation; iml, internal medullary lamina; Ip, interpeduncular nucleus; MB, mammillary body; MD, mediodorsal thalamic nucleus; MORE, Medtronic ANT-DBS therapy trial for epilepsy; mth, mammillothalamic tract; NBM, basal nucleus of Meynert; nth, nigrothalamic tract; OFCx, orbitofrontal cortex; pc, posterior commissure; PCG, posterior cingulate gyrus; PFCx, prefrontal cortex; PirF, piriform cortex, frontal division; pMCG, posterior midcingulate gyrus; Pt, putamen; PT, paratenial nucleus; pthi, inferior thalamic peduncle; PRt, prereticular zone; Pu, pulvinar; PV, periventricular thalamic nucleus; R, red nucleus; rcc, rostrum of corpus callosum; RSG, retrosplenial gyrus; RT, reticular nucleus; scc, splenium of corpus callosum; sm, stria medullaris; SN, substantia nigra; SNRp, posterior division of the pars reticulata; st, stria terminalis; thcg, thalamocingulate projection; tth, temporo-(pulvino-)thalamic tract; VAmc, ventroanterior thalamic nucleus, magnocellular part; vap, ventral amygdalofugal pathway; VAT, volume of activated tissue; VTA, ventral tegmental area.

* Corresponding author at: Moritz-Sommer-Str. 4, D-40225 Duesseldorf, Germany.
E-mail address: mai@uni-duesseldorf.de (J.K. Mai).

https://doi.org/10.1016/j.neuroimage.2022.119551.
Received 25 November 2021; Received in revised form 19 May 2022; Accepted 6 August 2022
Available online 7 August 2022.

1. Introduction

Deep brain stimulation of the anterior thalamic nuclei (ANT-DBS) has been established as an effective treatment strategy for the management of Drug-Resistant focal Epilepsy (DRE). It has demonstrated efficacy and is FDA and CE approved (Fisher et al., 2010; Salanova et al., 2015; Zangiabadi et al., 2019). The clinical benefit of the stimulation is, however, variable and with the current knowledge not reliably predictable with a median reduction of seizure frequency between 40% and 70% (Salanova et al. 2015). The MORE registry data support the effectiveness and safety of ANT-DBS therapy in a real-world setting in the years following implantation (MORE ClinicalTrials.gov Identifier: NCT01521754, first posted January 31, 2012). In the outcome evaluation of this registry the non-uniform positioning of DBS electrode in the ANT region was detected and it became clear that outcomes are not directly correlated to discrete positions in the ANT. Moreover, a substantial proportion of treatment resistant patients with seemingly optimally located ANT-DBS electrodes even failed to improve. Reasons for this failure to improve are supposed to be found either in patient selection, phenotyping, suboptimal stimulation strategies or peculiarities of a yet uncharted anatomical territory and a potentially very complex ANT region fiber network. This contribution set out to investigate the latter problem.

Mechanisms underlying DRE are explained by neurobiological factors (Schmidt et al., 2005) but also by altered spatiotemporal dynamics of functional connectivity and widespread structural changes (Cataldi et al., 2013; Bartolomei et al., 2017; Middlebrooks et al., 2017; Bernhardt et al., 2019). Many brain networks have been shown to have changed topologies in epileptic patients compared to controls. Functional networks implied the default mode network, the attention network and the reward/emotion network (Cataldi et al., 2013). The reported findings include globally increased and decreased connectivity (Pereira et al., 2010; Wirsich et al., 2016) or accompanying increased and decreased connectivity in neighboring networks (Bettus et al., 2008, 2009; Liao et al., 2010).

As a proposed mechanism, the altered functional connectivity in epileptic patients is modulated by ANT-DBS stimulation, which reduces the excitability in the Papez circuit (Zumsteg et al.,2006; Gimenes et. al. 2019). Successful ANT-DBS might produce increased connectivity of the default mode network (Middlebrooks et al., 2018) and importantly there is evidence that the patient correct positioning of the active contact within the ANT increases the probability of being a responder (Osorio et al., 2021). These findings hint at the significance of the patient-specific connectivity between the achieved ANT stimulation site and the epileptogenic network structures. Different parts of the ANT display different types of structural connectivity (Grodd et al., 2020).

So far, no position for active DBS contacts has been defined within the ANT or its immediate vicinity that unequivocally delivers seizure free results as sporadically reported for some individual cases (Osorio et al. 2021). Location of the optimal active ANT electrode contacts for different patient groups and epilepsy phenotypes may be at divergent positions in the ANT region (Fig. 1). The ambiguity of the position factor is underscored by the finding that mapping of the location of the active DBS contacts shows very close positions for different outcome groups (Majtanik et al., 2021) and indicates that the outcome of the stimulation might not depend only on the discrete subareas of the ANT subnuclei or on single cell populations. Positional factors for ANT-DBS influence the outcome variance explanation up to 22% (Krishna et al., 2016; Lehtimaki, 2016; Guo et al., 2020; Schaper et al., 2020). The relevance of moving the stimulation to the correct spot is further supported by the fact that "no benefit" patients can be converted to "responder" patients after reprogramming to a different electrode contact. Sometimes even a reimplantation of the electrodes (Järvenpää et al., 2020) is necessary. It might therefore not be satisfactory to place a DBS electrode into the ANT region. A patient and epilepsy-type specific position in a subregion of the ANT might therefore be a prerequisite for the optimal outcome.

The position of a Volume of Activated Tissue (VAT) by an active electrode contact determines not only its anatomical composition but also the specific pattern of activated networks. These findings emphasize the notion drawn in earlier studies that networks must be stimulated or otherwise influenced in order to contribute significantly to improved therapeutic (DBS) outcomes (Middlebrooks et al. 2018; Coenen and Reisert, 2021; Hu et al., 2021; Osorio et al., 2021). Whereas the dependency of the outcome of the stimulation from activated networks is hypothesized in this and other studies there exists neither an adequate topographically precise map of trajectories that potentially influence the human ANT region, nor the level of knowledge to explain how the projections are involved (and possibly compete) in the specific types of the epilepsy. This knowledge is indispensable for decoding the stimulation impact on the networks involved in the epileptic mechanisms.

Given that epileptic seizures are the consequence of a dysfunction of neural circuitry rather than the result of an etiologically isolated event (Zangiabadi et al., 2019) it must be considered that extrinsic fibers are activated by the active electrode in addition to the anatomical position of the ANT stimulation site. The proposition that the outcome of the stimulation depends on the activity of several competing ANT-related circuits necessitates the fine-grained analysis of the ANT region and the search for relations between the area directly affected by the stimulation with the brain regions to which this area is connected.

The structural network organization shows in animals a rather selective and segregated organization and there exists acceptable knowledge that also the human ANT has rather segregated source and target areas. That assumption lead us to expect that the better knowledge of the fiber organization in the ANT can be used to specifically influence the interaction between the epileptogenic zone and the ANT. The suspected dense fiber anatomy of the ANT region allows opposing networks for a distinct phenotype of DRE to reside in close proximity. A simulatenous stimula-

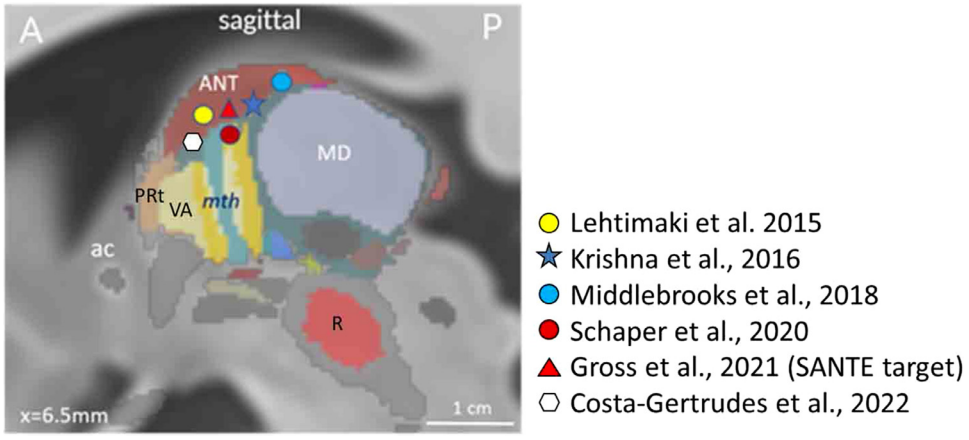

Fig. 1. Visual representation of distinct stimulation sites of the ANT-DBS responders in six published studies (listed above), overlaid on a paramedian section of MNI brain. For abbreviations see list of abbreviations.

tion of an epilepsy driving network together with an epilepsy dampening network might result in a non-effective stimulation. It is therefore conceivable that the stimulation effect in a suboptimal position for a certain patient might annihilate its own effect by such costimulation. To analyze several competing structures or networks affected in epilepsy we first of all aim to identify the fiber components in the ANT region and the direct ANT neighborhood, to disentangle their topographic relation with the ANT area and to understand their distant fiber relations in the context of knowledge about the pathophysiology of epilepsy. In order to increase the specificity of the delineated networks and to reduce the bias in tractography reconstruction we have applied a synthetic approach combining histology with tractography. From the results of the present study, we expect to gain information on how the stimulation in each position spreads across the extended three-dimensional fiber map of the ANT region. The resulting connectivity map is aimed to be later used for estimating of patient specific ANT connectivity and for optimization of the potential controllability of the patient specific epileptic network by the ANT-DBS stimulation. This whole concept needs to be fulfilled first of all in an anatomical setting of healthy subjects. For the moment such strategy reduces the complexity of the problem to identify fiber network subcomponents.

2. Materials and methods

2.1. Brain and imaging resources

A database of three high resolution diffusion Magnetic Resonance Imaging (dMRI) data sets was used to trace and reconstruct fiber bundles of the ANT region that were predefined on histological specimen. The dMRI data sets from the *ex-vivo* specimen included a complete brain without record of neurological or psychiatric diseases and fixed in formalin (10T, 0.66mm voxel size) from the body donation program of the Dept. of Anatomy of the University of Duesseldorf and a brainstem (200 µm voxel size) approved by the Duke University Health System Institutional Review Board (Calabrese et al., 2015; Adil et al., 2021). In addition, we used Human Connectome Project data (7T diffusion data, 1.05 mm voxel size).

2.1.1. Post-mortem *brain*

For the *post-mortem* whole brain single-shell high angular resolution diffusion imaging (HARDI) data were acquired with 64 unique diffusion directions at $b = 5{,}000$ s/mm^2 and 8 $b = 0$ s/mm^2 ($b0$) volumes. The T1w and the T2w scanning resulted in a 332 µm isotropic voxel size anatomical 3D images with $512 \times 512 \times 360$ size. Total acquisition time was 15 h.

For the anatomic images, a 3D gradient echo pulse sequence with repetition time (TR) = 50 ms, echo time (TE) = 10 ms, flip angle (α) = 60 degree, and bandwidth (BW) = 78 Hz/pixel was used with a total acquisition time of 14 h

2.1.2. Brainstem

The brainstem dMRI data set was compiled from a 65-year-old anonymous male subject with no history of neurologic or psychiatric disease. Before it was transferred to a custom-made MRI-compatible tube it was immersion fixed and doped with 1% (5 mM) gadoteridol (ProHance, Bracco Diagnostics, Monroe, Township, NJ). The MR images were acquired with a 7 Tesla small animal MRI system using a 65 mm inner-diameter quadrature RF coil (M2M Imaging, Cleveland, OH) for RF transmission and reception.

The diffusion data were acquired using a simple diffusion-weighted spin echo pulse sequence (TR = 100 ms, TE = 33.6 ms, BW = 278 Hz/pixel) with a total acquisition time of 208 h. A pair of unipolar, half sine diffusion gradient waveforms of width (δ) = 4.7 ms, separation (Δ) = 26 ms, and gradient amplitude (G) = 50.1 G/cm was used for diffusion preparation. High angular resolution diffusion imaging (HARDI) data, single-shell, were acquired with 120 unique diffusion directions at b = 4000 s/mm2 and 11 b = 0 s/mm2 (b0) volumes distributed evenly during the acquisition. The FOV was $90 \times 55 \times 45$ mm. The acquisition matrix was $450 \times 275 \times 225$ produced a scan with 200 µm isotropic voxel size.

2.1.3. Human connectome project

The data from the Human Connectome Project (HCP) derived from subjects scanned with 7T MRI (HCP-1200 release (Glasser et al., 2013; Van Essen et al. 2013). The data of 10 subjects with the full MRI acquisition pipeline of 2 structural, 4 resting state, 7 tasks and 1 DWI session were selected (for complete scanning protocols for each 7T imaging session see http://protocols.humanconnectome.org/HCP/7T). We selected 5 male and 5 female subjects in the age range of 22–37.

2.1.4. Immunohistochemical sections

The immunohistochemical sections derived from brains collected and examined since 1989 by the University Departments of Neuroanatomy and Neuropathology at Düsseldorf and of Pathology in Mainz, observing the local Ethical Committee protocols in all cases. Procedures for collecting material were in accordance with the ethical guidelines of the Helsinki Declaration regarding informed consent (World Medical Association, 1996). Neuropathological examination of the tissue yielded no evidence of CNS malformations or abnormal structural changes of the brain on either gross examination or microscopic analysis.

Summary of resources used for analysis:

1	*Ex-vivo* specimen (one healthy brain N=1), fixed in formaline and scanned over 15 h in a 10T scanner at 0.66 mm voxel size
2	*Ex-vivo* brainstem (one healthy 65- yo, N=1) immersion-fixed in a tube, scanned over 208 h in a 7T MRI at a 0.2mm voxel size
3	The HCP-1200 release data set (N=10)
4	Immune histochemical sections derived from brains collected in the Dept. of Neuroanatomy, Duesseldorf, Germany

2.2. Neuroanatomical substrate and anatomical priors

An abundance of fibers within and around the ANT forms an intricately distributed network with differing fiber densities and orientation. Assuming that the DBS stimulation effect varies as a consequence of the activation of different fiber bundles or networks we developed a high-resolution fiber atlas of the ANT region in tree steps:

1 Selection, discrimination and tracing of significant fiber components on microscopic sections to map the connectivity of the ANT region. This step is based on the knowledge about the structural organization in humans augmented by comparative anatomical studies in animals and clinico-pathological studies in *post-mortem* brains. This step results in a set of anatomically defined fiber bundle priors that will be used in the next step.
2 Estimation of the preliminary structural connections of the ANT by probabilistic tractography and creation of seeding masks and tract selection volumes
3 Synthetic Pathway Reconstruction (SPR) by iterative combination and refinement of the results from the histological data (anatomical priors) with the virtual fiber components from tractography.

2.3. Selection of the ANT associated fiber bundles

The fiber bundles selected for the structural connectivity map are either directly connected with the ANT or are topographically closely related and therefore affected by an active DBS contact (Fig. 2). Many connections are known to be implicated in the complex epileptogenic network (Deppe et al., 2008; Chen et al. 2020). Some pathways of this network are well circumscribed and thus easily demarcated. Others are only delimited on the basis of tedious analysis that also includes immunohistochemistry and the study of developmental processes when

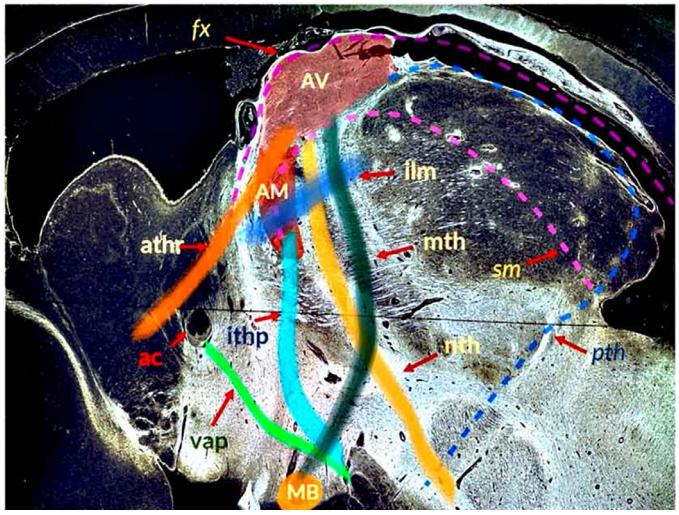

Fig. 2. Schematic depiction of the orientation of fiber systems related to the ANT (paramedian section, anterior is to the left). The darkfield image shows neurofilament 200 positive fibers in white, non-immunoreactive fibrous tissue appears in black. The coloured lines indicate the main orientation of fibers related with AV and AM. The dashed lines are 3 projections of the pathways not directly visible in the slice. For abbreviations see table 2 below.

Table 1
Fiber bundles selected for the synthetic pathway reconstruction of the ANT region.

Extended hippocampal system (Papez circuit)		
Input:	fornix (pre- and postcommissural division)	*fx*
	temporo-(pulvino-)thalamic fibers	*tth*
	mammillothalamic tract	*mth*
Output:	ANT-cingulate projection	*thcg*
	anterior route	*thcg-a*
	posterior route (stratum zonale)	*thcg-p*
Extended amygdaloid system		
	stria terminalis	*st*
	ventral amygdalofugal pathway	*vap*
	inferior thalamic peduncle	*ithp*
Orbitofrontal system		
	anterior thalamic radiation	*athr*
Dorsal diencephalic conduction system		
	stria medullaris thalami	*sm*
	habenulo-interpeduncular tract	*fr*
Others		
	Internal medullary lamina, anterior division	*iml*
	Nigrothalamic fibers	*nth*

the specific maturation period discloses the characteristic organization. Many components that were well described using experimental procedures in animals have not been adequately replicated in humans, e.g. the segregated projection of the *mth* or the course of the thalamocingulate fibers. The fiber bundles included in our analysis are listed in table 1.

Extended hippocampal system (Papez circuit): The ANT represents a most important subcortical node within the "classical" hippocampal–anterior thalamic-cingulate circuit. We included additional fibers connecting subcortical structures defined as the "extended-hippocampal system" (Aggleton et al. 2010). This comprises besides the hippocampal formation (dentate gyrus, CA fields, and the subiculum) also constituents in the basal forebrain and tegmentum.

The **extended amygdaloid system** comprises the circular and basal fiber arrangement that connects the amygdaloid nucleus with the bed nucleus of the stria terminalis (BNST, Alheid et al., 1990; Alheid. 2003). The BNST is grossly organized around the anterior commissure as a complex conglomerate of subnuclei with rather precise margination revealed by their immunohistochemical characteristics (Walter et al., 1991).

The stria terminalis is the dominant efferent pathway with a segregated fiber composition (Johnston, 1923; Post and Mai, 1980) from the amygdaloid nuclei in rodents. It is greatly reduced in primates in favor of the basal subpallidal analogue, the ventral amygdalofugal pathway (Pabba, 2013). In humans, the mostly very fine fibers of the stria terminalis are recognized as a circular band lying in the terminal sulcus medial to the caudate nucleus and adjacent to the thalamostriate vein.

The basal fiber arrangement of the ventral amygdaloid pathway also connects the amygdala with (mainly) the bed nuclei of the stria terminalis. At the very narrow passage way in the sublenticular continuum these fibers are separated from the inferior (ventral) thalamic peduncle by the basal nucleus but both fiber systems are very difficult to distinguish as they reach the thalamus. We have therefore included the inferior) thalamic peduncle within the extended amygdaloid system.

Orbitofrontal system: The ANT nuclei are connected with certain parts of the prefrontal and orbitofrontal region by the anterior thalamic radiation which is part of the anterior limb of the internal capsule (*alic*). *Alic* is a heavily myelinated composite bundle that carries fibers between the thalamus and the frontal cortex, the anterior cingulate and also the temporobasal areas (mainly the medial prefrontal cortex). *Alic* also contains the frontopontine tract, bidirectional thalamostriate fibers and fibers to the ventral tegmental midbrain (Ongür and Price, 2000; Coizet et al., 2017). *Alic* shows a coarse topological organization with segregated ventrodorsal and mediolateral partitions (Safadi et al., 2018). We have analysed the fibers connected with the AV and AM differently.

The **dorsal diencephalic conduction system** (Sutherland, 1982) connects limbic forebrain with limbic midbrain structures circumventing the hypothalamus. These latter nuclei in turn give rise to the habenulo-interpeduncular tract (fasciculus retroflexus) that connects with the highly cholinergic interpeduncular nuclei. The stria medullaris fibers course as a well marginated myelin-rich bundle lengthwise along the dorsomedial margin of the thalamus between the anterior pole of the thalamus, the „stria medullaris bed", and the habenula, exchanging fibers with the ANT. Ventrally to the ANT the fibers cannot longer be distinguished from those of the stria terminalis (Fig. 16 a).

The **internal medullary lamina,** *iml,* was described as "great defining landmark" (Jones, 1998) because it separates as a fiber-rich partition the anterior, medial and lateral region of the thalamus. This territorial distinction is visible in regular MRI and can be used for localizing the ANT. Among the three divisions of the *iml* (Mai and Forutan, 2012) only the anterior part has intense fiber exchange with the ANT.

Nigrothalamic fibers: The efferent GABA-ergic fibers from the (posterior) substantia nigra pars reticulata (SNRp) reach the ANT alongside of the *mth* passing through the intralaminar formation lateral to the mediodorsal nucleus (Carpenter and Peter; 1972; Mai and Forutan, 2012).

2.4. Production of the anatomical high resolution fiber map integrated within the MNI space

Creating an anatomically accurate map of the fiber pathways of the ANT region requires consistent anatomical materials and detailed anatomical knowledge about the specific features of each pathway. We used anatomical fiber priors, the 3D volumetric representation of pathways in a dense stack of aligned brain sections (histological or high-resolution MRI).

Step 1: Anatomical pathway priors

For the construction of the anatomical fiber map priors we relied on two brain atlases representing either hemisphere of one young individual (Atlas of the Human Brain, AHB4, right hemisphere and MRX-Atlas, left hemisphere, Fig. 3a) that are represented in the native space and in the MNI space (Fig. 3 b). To represent each pathway with the

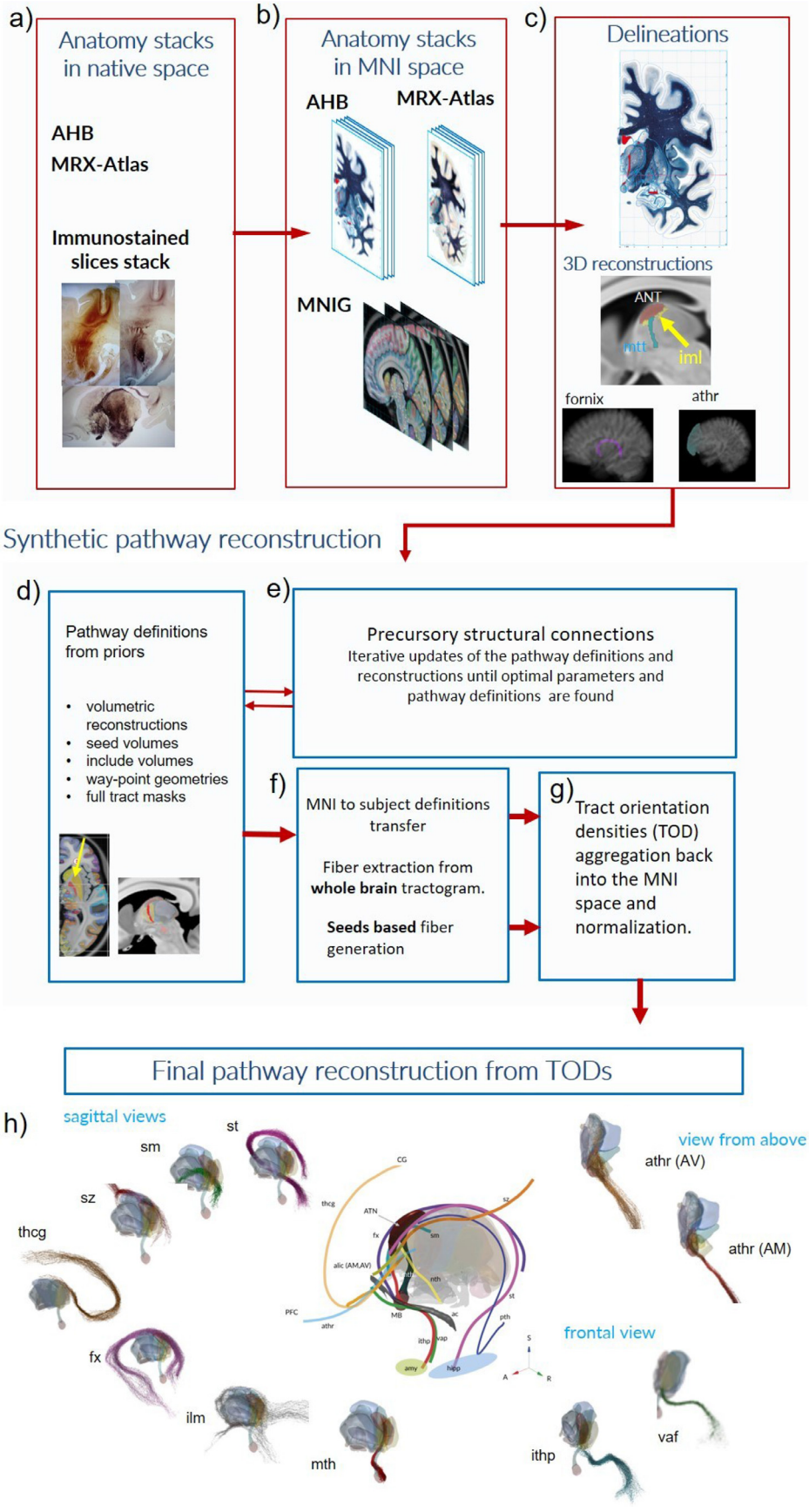

Fig. 3. Process of synthetic pathway reconstruction. (a) Histological information and atlas parcellations were tranferred to single slices in native space and converted to path masks. (b) Transfer of the path masks into the MNI slice stacks. (c) 3D reconstruction of the tracts from the dense slice stacks. The lower images show 3D pathway priors for the fornix and athr in the MNI brain. (d) Creation of ANT region pathway definitions. (e) Construction of precursory pathway trajectories followed by an update of the pathway definitions. (f) Seed regions include volumes and pathway masks transfer from MNI to subject space and pathway extraction. (g) Aggregation of Tract Orientation Densities (TOD) in MNI space. (h) Finalized pathways visualized with MRX Atlas brain structures. The center grid schema aggregates the pathways in an orientation of structures not standard for each structure, but optimized for viewing.

requested detail objectivity and distinctiveness, we added information obtained from archival immunostained sections. Most valuable were sections of immature human brains because early and later maturing pathways can be distinguished selectively by applying histochemical methods (Ashwell and Mai 2012; Mai and Forutan, 2012). For the parcellation of the various fibers we used fiber density, compactness, orientation, neighborhood relation and histochemical properties. The segmentation of the immunostained serial sections were carried out by an expert neuroanatomist and manually transferred to the brain stacks containing Nissl- and Weigert-stained microscopic slices of the AHB4 and the "MRX-Atlas" in native space respecting neighborhood relations with general and topometric characteristics of the studied region (intervening fibers, neuronal populations, chemical features and characteristics derived from development, distance values).

The versatility of the priors was boosted by registration of the stack slices into the MNI space. Such normalized stacks of sections representing a space with defined coordinated system (origin of the MNI and its main axes) served as an unambiguous reference for anatomical representation available for many alternative processing pipelines. The native Atlas stacks transformation into the MNI space (ICBM/MNI_2009b) was performed by a geometrically constrained Atlas normalization procedure (Mai et al. 2015, Mai and Majtanik, 2017., Mai and Majtanik 2017).

The pathway reconstruction procedure operates on the data of dense slice stacks containing three atlases registered in the MNI space (AHB4, MNIG, MRX-Atlas) and the imformation from the immunostained sections. The compilation of all parameters representation of each parcellated tract embedded in the two atlases resulted in a 3D pathway reconstruction (first anatomical priors, Fig. 3 c). The segmentation strategy was iteratively checked in the atlas representation at any further step of our analysis and, if necessary, revised according to the available landmarks and distances relations. Immunostained (serial) sections or scans (derived from the available brain collection) that display morphochemical properties of each pathway of interest were delineated at meso- and microscale resolution.

These manually segmented and reconstructed anatomical priors of the tracts and fascicles of interest provided an anatomically approximating representation of their anatomical organization related to the ANT.

Step 2: Estimation of the precursory structural connections of the ANT by probabilistic tractography, the creation of seeding masks and of tract selection volumes.

In this step we generated a test set of ANT pathways to ensure that the tractographically reconstructed pathways follow the anatomical priors. If discrepancies appeared we changed the paramenters and updated the priors.

At first a default set of pathway definitions for tractographic reconstructions was generated from the precursory anatomical priors (Fig. 3 d). The pathway definitions consisted of the 3D volumetric representation of each pathway, selection-volumes (waypoint volumes) for fiber selection and pathway masks for spatial extent control of the tracts. In this step we also tested which values of the tractography parameters (cutoff, maxlength, minlenght, angle) yielded the best results.

From the anatomical priors in the MNI space, we manually determined two volumes for each pathway: one closest to the ANT, the other farthest distally where the tract was anatomically determined (in the MNI space). The pathway definitions were transformed to the individual brains by inverse deformation fields resulting from the normalization of the subject brains into the MNI space.

For the ten HCP brains, the post-mortem brain and the brainstem, a global tractography within the constrained spherical deconvolution framework (CSD) was computed. For each pathway we selected all tracts passing through the two selection volumes. We visually checked if the resulting tracts correspond to the pathway priors. In the cases of major deviations we augmented the selection volumes or used volumes of avoidance (for example *ithp*).

For many tracts the global tractography as outlined above did not result in the expected unambiguity compared with the anatomical concept. These included the thalamocingulate projection (*thcg*), temporo-(pulvino-)thalamic fibers (*tth*), fasciculus retroflexus (*fr*), stria medullaris (*sm*) and the nigrothalamic fibers (*nth*). For these tracts we employed seed-based tractography and performed additional iterations of constructions of the seed and selection-volumes, enhanced by regions of avoidance to ensure that the resulting tracts fit the anatomical priors. The seed based tractography used a dilated volumetric representation of the tract, the tract mask, which was larger than the region through which the tract will pass.

Step 3: Synthetic pathway reconstruction (SPR)

For the final 3D characterization and documentation of the axonal pathways connecting the ANT region with other components of the human brain, we used a synthetic pathway reconstruction approach (Fig. 3 d-g).

The SPR utilizes the updated anatomical fiber map priors from step 2 for the definition of pathways reconstructed from the diffusion MRI data (Fig. 3 d). This approach relates the actual histological individual fibers/connectivity priors to the virtual *in-silico* fiber pathways/connectivity patterns generated with tractography. The methodology applied iterative refinement of histologically verified trajectories and source/target definitions with high resolution anatomical tractography (Fig. 3 e). The reconstructed axonal trajectories of the ANT region were synthetically assembled into a 3D model of the fiber pathways related to the ANT region (Fig. 3 h).

The first step of the SPR used the anatomical pathway priors to generate a set of pathway definitions for tractographic reconstructions (Fig. 3 d). The pathway definitions consisted of 3D volumetric representations, seed and way-point volumes for fiber selection and pathway masks for spatial extent control of the tracts. With these pathway definitions, we tractographically reconstructed the 12 bundles that were mapped on the microscopic slides. The alignment of these reconstructions with the anatomical priors was then used to adjust and optimize the pathway definitions and tractography parameters in order to ensure the anatomical plausibility and completeness of the reconstructed pathways (Fig. 3 e).

After the final update cycle, the pathway definitions were transferred from the MNI to the subject spaces and corresponding fibers were extracted from the whole brain tractograms and normalized to the MNI space by nonlinear deformation fields (Fig. 3 f). For each pathway the tracts were scaled with the corresponding SIFT2 coefficients (Spherical-deconvolution Informed Filtering of Tractograms) to obtain an estimate of fiber densities (Smith et al., 2015). Further, the tract orientation densities (TOD) were computed and aggregated into the MNI space (Fig. 3 g). Probabilistic tractography with dynamic seeding was performed on the normalized track orientation densities to obtain final representations of the pathways. During this process, however, the final fiber bundles did not retain the quantitative properties contained in the individual SIFT2 coefficients (for details see Supplementary information). The sum of the pathways that were generated by the iterative refinement of the tractographic reconstructions with the histological priors resulted in a complex high-resolution fiber map of the ANT region, that we name a 3-D "fiber grid map".

The registration of the probabilistic tractography back into the Atlases (Mai et al., 2015; Mai and Majtanik, 2017; Mai and Majtanik, 2010; Mai and Majtanik, 2019) provides the correspondence between the pathways and the histological trajectories. The result is consistent with existent knowledge and more selective with respect to histological detail and topographic precision than recent DTI results in humans (Grodd et al., 2020). Since this study is aimed to correlate fiber pathways with study group data, we did not distinguish between subnuclei in most instances.

2.5. Aggregation of the scans into the MNI space

All scans were combined by normalization into the MNI space in a high resolution registration pipeline with geometric shape constrain (Mai et al. 2015). The pipeline performs a sequence of rigid, affine and non-linear whole brain multi-spectral registrations with an additional channel containing the geometrical constrains. A single geometric shape constrain defines a homologous structure in the AHB and in the MNI brain that will be perfectly matched during the nonlinear part of the registration process. The geometric constrain can be defined as a set of one-, two- or three-dimensional structures (1D, 2D or 3D constrain). The pipeline enforces perfect match of the geometrical constrains. The constrains defined were: *mth, ac, pc*, fornix, ventricles, corpus callosum, optic tract, lateral and medial geniculate bodies, septum, mammillary bodies.

The anatomical priors were defined in the MNI space and transferred into the individual subject space by warping operation utilizing the inverse of the transformation fields. The priors were then smoothed in the individual space and used for the selection of the tracts from the global tractography into a tract bundle. To be selected and included from the tract we required that fibers have to be inside the smoothed prior volume.

2.6. Processing of the imaging data

The anatomical scans and the dMRI data were processed with our MRX-Brain ANT pipeline that uses the CSD tractography framework (Tournier et al. 2004, 2007, 2012) of the MRtrix3 software (https://github.com/MRtrix3/mrtrix3). The MRX-Brain ANT pipeline performs precise segmentation of the subcortical structures and normalization of the T1 images to the MNI space. Prior to the processing of the DWI data the anatomical image in the native space was segmented into tissue types (GM, WM, CSF, …) and converted into the 5TT (five tissue type) file format, that is used for Anatomically Constrained Tractography (ACT) by the MRtrix3 (Tournier et al. 2012,Smith et al., 2012).

The processing and the tractographic reconstruction from the DWI data were carried out using functions from the MRtrix3 software package (Tournier er al., 2019). The DWI data were subjected to multi-tissue multi-shell constrained (msmt_5tt, msmt_csd) spherical deconvolution for the HCP and brainstem data, and multi-tissue single shell for the postmortem whole brain data. The HCP full brain and the brainstem tissue response functions were reconstructed with the multi-shell multi-tissue tractography option (msmt_5tt) of the dwi2 response mrtrix3 command and masked with the whole brain mask. The postmortem full brain tissue response functions were estimated with the multi-tissue single-shell option (msmt_csd) and masked with the whole brain mask.

Whole brain probabilistic tractography was performed using the iFOD2 algorithm implemented in the tckgen mrtrix3 command. In the CSD framework, the fiber tracking works by advancing along a particular direction at each tracking step. The probabilistic algorithm works on a Fiber Orientation Distribution (FOD) image represented in the Spherical Harmonic (SH) basis. The step direction is computed by sampling the FOD of the current position. A streamline is more probable to follow a path where the FOD amplitudes along the path direction are large; but it may also rarely traverse orientations where the FOD amplitudes are small, as long as the amplitude remains above the FOD amplitude threshold along the entire path.

Whole brain probabilistic tractography for the HCP data and for the full postmortem brain was performed with the options: -cutoff 0.06, -minlenght 3, maxlenght 200, angle 35 and -seed_dynamic from the white matter normalized FOD data. Total of 50 million tracts for each subject were obtained.

For the brainstem the parameters were: cutoff 0.04, -minlenght 3, maxlenght 100, angle 35 and -random seeding from the whole brainstem. Total of 10 million tracts were computed.

For quantitative analysis of connectivity strength and for further optimization the weighting values of the tracts were computed with the “Spherical-deconvolution Informed Filtering of Tractograms” algorithm (SIFT2, Smith et al., 2015). The algorithm estimates appropriate cross-sectional area multiplier for each streamline to establish a quantitative measure of fiber density. The weights are optimized such that the reconstructed fiber volumes match those estimated directly from the diffusion signal throughout the brain white matter. The estimation of quantitative structural connectivity between two areas can be computed by using the SIFT2 algorithm cross-sectional areas weights for each streamline. During the pathway reconstruction process, however, the final fiber bundles did not retain the quantitative properties contained in the individual SIFT2 coefficients. Therefore quantitative measurements of the connectivity were not possible.

The SIFT2 based tractography, however, was not able to reconstruct some of the tracts. For these tracts different strategies were employed to achieve optimal reconstruction. The alternative strategies included iterative definition of the seed and waypoint regions that were optimized by regions of avoidance to ensure that the resulting tracts fit the anatomical priors.

The seed based tractography uses a dilated volumetric representation of the tract, the tract mask, which was larger than the region through which the tract will pass. The seeds were randomly selected from the positions inside the tract mask volume. The tracts were computed with the same parameters as the global tractography, except that the maxlength parameter was adjusted to be slightly longer that the estimated tract length. All computed tracts had to pass all defined selection-volumes. The number of computed tracts was adjusted in such a way that at least 100 tracts could be selected for the final tracts.

In most cases, predefined regions from our volumetric tract reconstructions were optimal for ROI, waypoints and stop region definitions and only in few cases new ROIs were constructed to serve as additional waypoints guiding the tracts in anatomically correct directions.

The tracking was done in the subject space where the track orientation densities were computed and then warped into the MNI where the final tracts were computed on averaged group TODs.

The Tract Orientation Density (TOD) maps for each pathway were obtained by the tckmap map command with the tod=12 option and 0.7 mm resolution. The TOD maps were then warped into the MNI standard space with the mrtransform MRtrix3 command and the reorient option turned on. The warp transformation used the deformation fields obtained from the registration of the T1 and T2 images. The TOD maps were then averaged across subjects and normalized. The TOD maps in MNI standard space in such way were then used for probabilistic pathway-specific tractography using iFOD2 algorithm with a moderate stopping criterion (cuttoff value 0.005). The minlengh and maxlength values were adjusted (-20% and 20% offset) with respect to the estimated length of the pathway priors

Further refinement was carried out with working pathway definitions and tract generation processes to trim away erroneous tracts (false positives) to retain the most accurate fiber bundles. To this end the expert knowledge of the authors and the assembled anatomical prior database was used to clean up the fiber bundles. The final tracts were then visualized overlayed onto the 3D thalamus.

3. Results

Our analysis showed that histological and tractographic data of the fiber bundles in the common space can be combined in spite of the rather small territory of the ANT subnuclei and the different scaling of the images obtained by these approaches. Fig. 4 shows that slight shifts in the seed point locations result in significant differences in the course of the connections. If seed points are placed in areas roughly corresponding to the ANT subdivisions different connectivity profiles are observed. This finding, which matches descriptions in the literature, shows that a pattern of pathways may be obtained also with tractography that can be

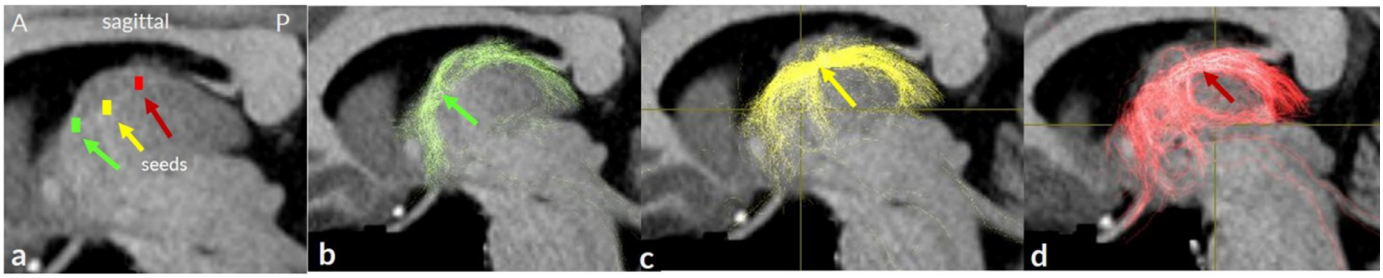

Fig. 4. Tractograms of subareas of the ANT region (colored squares) derived from diffusion MRI of a HCP subject overlaid on a T1 image. The first sagittal image (a) shows the three different seed volumes used. The images b-d show that seed positions in different subareas of the ANT (left row) result in unequal trajectories and demonstrate the feasibility of distinguishing segregated pathways emanating from subnuclei of the ANT.

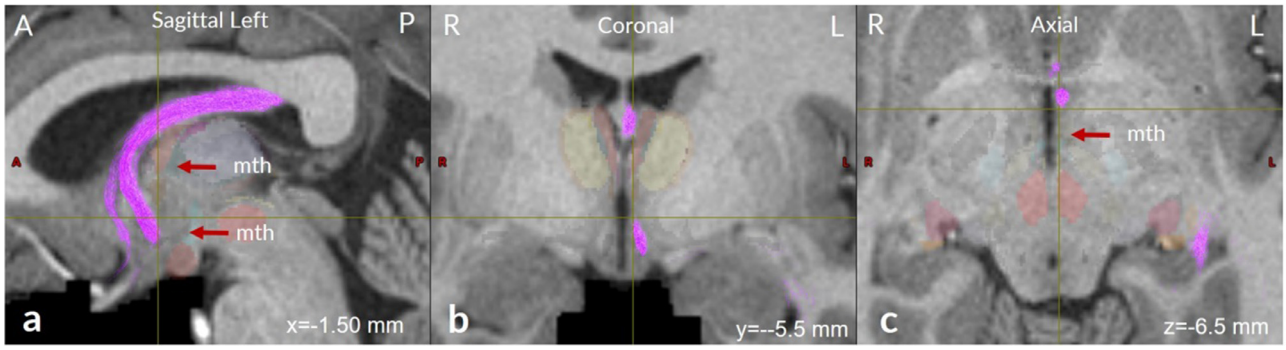

Fig. 5. Tractograms showing the extension of the fimbria-fornix system (fornix: lilac; mth: blue) in a T1 scan. The parasagittal view shows the distinct precommissural fornix component extending to the basal forebrain (a). The coronal view highlights the fornix entry zone at the mammillary body.

easily matched to the histological resolution. This example shows how slightly individual divergences of electrode positions (or stimulation settings) change the composition of the fiber structures affected.

With the view that several competing structures and networks are affected in epilepsy, we aimed to determine what fiber components are organized in ANT and its direct neighborhood to disentangle their topographic relation within the ANT area and to understand their distant relations in the context of knowledge about the pathophysiology of epilepsy. Figs. 2 and 4 display the high complexity of fiber bundles selected and their coarse orientation. The fiber systems included are listed in Table 1.

3.1. Extended hippocampal system (Papez circuit)

The ANT is a crucial node within the hippocampal–anterior thalamic-cingulate circuit and most important for the understanding of seizure origin, propagation, or expression (Samadani and Baltuch, 2007). We looked at these components with detail and compared some characteristics with findings in experimental animal studies.

3.1.1. Afferent fibers

The ANT receives its input from subareas of the hippocampal formation. The predominantly glutamatergic afferents reach the ANT either directly via the fornix (Percheron, 2004) or indirectly from the fornix after relay in the mammillary nuclei by the mammillothalamic tract, *mth* (Gonzalo-Ruiz et al., 1996; Bernstein et al. 2007; Dillingham et al., 2015). The pre- and postcommissural fornices are reliably demonstrated (Fig. 5) as is the *mth* which presents as a compact bundle that is related only with AV (Fig. 6).

A larger and circumscribed share of the fornix column separates as precommissural fornix above the anterior commissure to reach the limbic forebrain area (Fig. 5). This is a compelling difference to the course of the fibers shown in the immunostained section (Fig. 7). It is explained by the partial volume effect misrepresenting the thin septum pellucidum in the MRI. The characterization is relevant because the septal area is the source of several efferents to the hippocampus and exchanges fibers with the stria terminalis and the stria medullaris (see below).

The predominance of the mentioned *mth*-afferents to the ANT shall not provoke to neglect other sources of direct relations within the extended hippocampal (limbic) system. That includes fibers from the entorhinal region which do not join the fornix but take an alternative route to reach the anterior (limbic) nuclei. These fibers were described as temporopulvinar (or temporothalamic) bundle (Whitlock and Nauta, 1956; Krieg, 1973). Fig. 8 shows the fiber stream with its relations with the entorhinal cortex region, the course around the inferior horn of the lateral ventricle and along the perimeter of the pulvinar in the external medullary lamina until the dorsal superficial nucleus with fibers reaching AV.

3.1.2. Efferent fibers

The output of the ANT forms part of the thalamo-cingulate projection (*thcg*) and target the limbic lobe on the internal surface of the hemisphere. The fibers innervate the cingulate and retrosplenial cortex. They join the cingulum bundle which also contains association and callosal fibers. We distinguished two routes to the cingulum bundle. An anterior fiber stream (*thcg-a*) travels forward and assembles between the medial wall of the hemisphere and the lateral ventricular area to reach the anterior cingulate area (Fig. 9). They do not use the passage through the anterior limb of the internal capsule but follow a more medial course (Fig. 9 c,d). Interestingly, the streamlines are followed until only in the anterior (genual) and the anterior middle cingulate cortex.

The other, posterior trajectory (*thcg-p*) consists of fibers that leave the ANT in the stratum zonale. These fibers traverse the centrum semiovale, penetrate the corpus callosum and join the callosal bundle. This relation is verified in the clinico-pathological case (Fig. 10) where the loss of interfering myelinated axons allows tracing the fibers between the ANT and the cingulate gyrus. The well myelinated fibers of the stratum zonale turn around the occipito-frontal association bundle before they perforate the callosal fibers to reach the limbus of the hemisphere (the base of the telencephalic evagination). Our material was unsuited to follow fibers

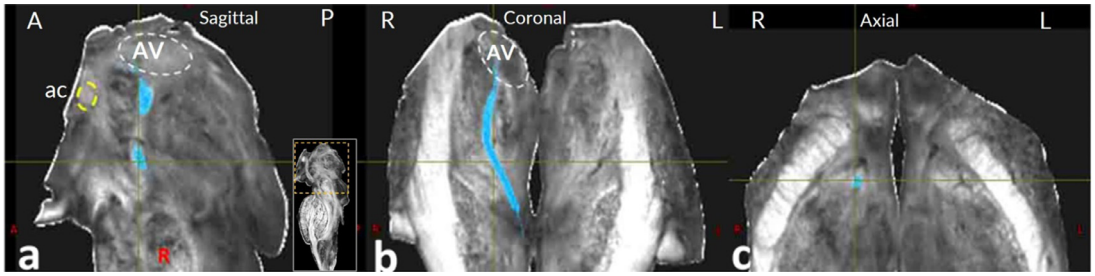

Fig. 6. Demonstration of the mammillothalamic tract (blue) without any indication for a relationship of the tract with other than the AV nucleus (yellow broken line: anterior commissure (ac); white stippled outline: AV). The sagittal, coronal and axial sections are cut perpendicular to the brainstem axis of Meynert. The navigation box in the right lower corner of (a) shows the orientation of the brainstem scan.

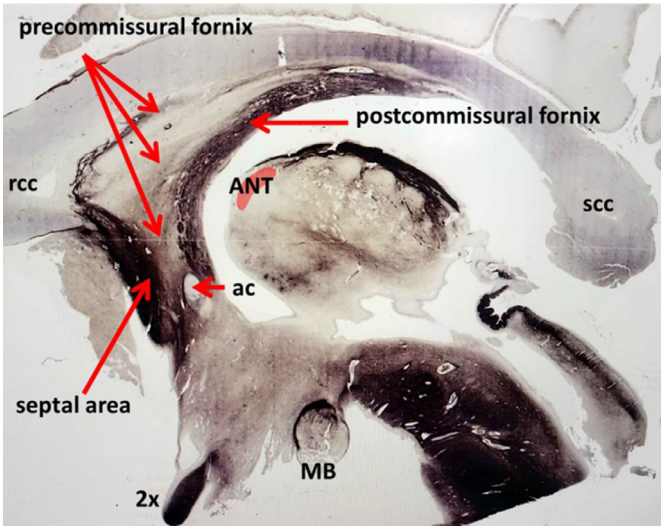

Fig. 7. Paramedian section at perinatal age showing SMI-312 immunoreactive fibers. A considerable amount of the precommissural fornix fibers course below the anterior corpus callosum whereas those separating immediately above the anterior commissure are shown with minor intensity. The image thus illustrates the structural separation between the postcommissural (excitatory) and precommissural (mostly inhibitory) fornix fibers. Note the appreciable extension of the interventricular foramen separating the fornix from the ANT (marked in red). For abbreviations see table 2.

to the orbito- and prefrontal cortex anteriorly and the parahippocampal gyrus posteriorly, respectively.

In the tractogram the cingulate fibers are rather loosely grouped and can be followed in anterior and posterior directions to the middle and retrosplenial segments of the cingulate region (Fig. 11 a,c).

Within the cingulate gyrus the afferents were described to be located in the basolateral portion of the medullary core (Mufson and Pandya, 1984) which is compatible with the trajectory shown in Fig. 11. They are separate from the dorsolateral and dorsoventral sectors of the cingulate cortex where the corticofugal (cingulothalamic) and associational (callosal) fibers are located (Domesick, 1970)

3.2. *Extended amygdaloid system*

Both components of the extended amygdaloid system, the stria terminalis and the ventral amygdalofugal pathway are easily recognized. The **stria terminalis** (*st*) is identified as a conspicuous band of fibers from the amygdala along the terminal sulcus to the bed nuclei of the stria terminalis (BNST) situated around the anterior commisure. Considering the rather loosely arranged fibers embedded within the glial rich substance of the caudothalamic groove the markedness of the streamlines in humans is conspicuous (Fig. 12).

The complex projection field of the *st* is reflected by the widely marked area comprising the conglomerate of subnuclei of the BNST and also extensive parts of the hypothamus marked by the postcommissural fibers.

The **ventral amygdalofugal pathway** (*vap*) presents as a continuum that extends between the central (and basolateral) amygdaloid cell groups with the medial and lateral nuclei of the septum and the BNST (Nauta and Haymaker, 1969). We were interested only in the portion that was originally defined by the demonstration of cholinergic fibers (Fig. 13 c). This division partly overlaps with the **inferior thalamic peduncle** (*ithp*) at the subpallidal segment. As shown in Fig. 14 both fiber bundles have different orientations with respect to the frontal plane and are separable medially where *vap* reaches the BNST whereas the *ithp* innervates the limbic thalamus. *Ithp* is a composite bundle (Klingler and Gloor, 1960; Riley, 1960) that recruits its afferents mainly from the amygdala and the basal, insular and anterior temporal cortical regions. The fibers then become rather compact and curve dorsally around the medial margin of the emerging pallidal fibers to enter the polar reticu-

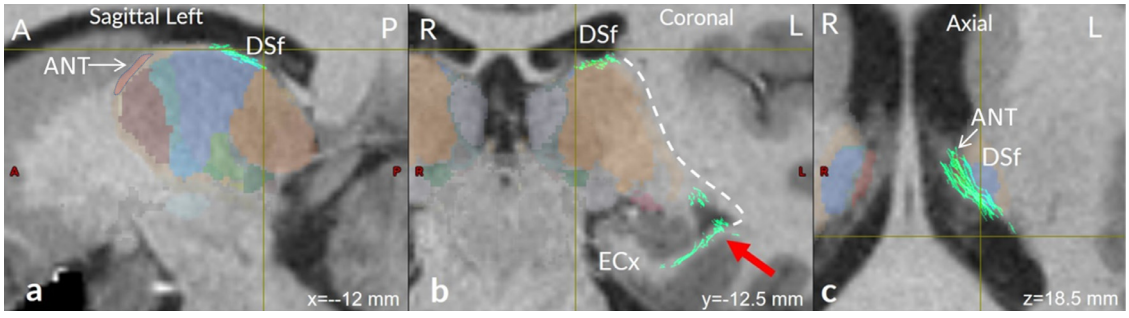

Fig. 8. Trajectory determined for the alternative pathway connecting the entorhinal cortex with the anterior thalamic nuclei (dorsal superficial nucleus, DSf and ANT). Sagittal (a), coronal (b) and axial (c) views in a T1 image. The arrow indicates the connection between the entorhinal cortex and the base of the ventricle.

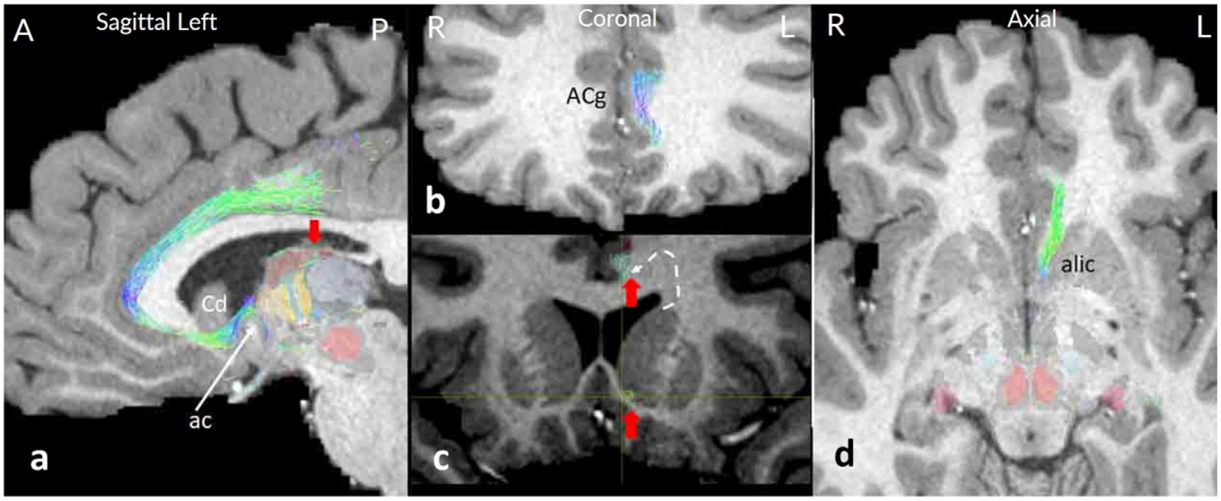

Fig. 9. The trajectory of the anterior thalamo-cingulate fibers and its distribution along the anterior and middle cingulate cortex. The fibers emanate from the ANT in anterior direction and course around the genu and rostrum of the corpus callosum to extend above the corpus callosum in the basolateral cingulate gyrus. The location of fibers depicted in the frontal and axial images (T1) is outside the *alic*.

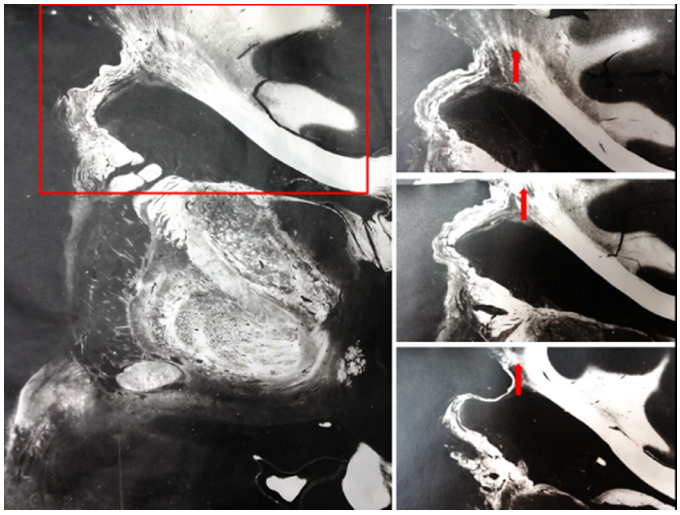

Fig. 10. Coronal sections showing the core of the left hemisphere in a case of middle cerebral artery infarction (Weigert stain). Insets on the right show the boxed area at further caudal levels. Whereas in normal preparations the fibers in the stratum zonale are impossible to follow further distally because of the multiple fiber orientations at the centrum semiovale the massive loss of fibers allows following them to the cingulum bundle (arrow). These fibers bend around the caudate nucleus along the occipito-frontal association bundle before they perforate the callosal fibers to reach the limbus of the hemisphere.

lar thalamic nucleus (Ncl. fasciculosus) where the fibers fan out towards their destination in the MDmc and AM.

3.3. Orbitofrontal system

The anterior thalamic radiation (*athr*) connects the ANT nuclei with the prefrontal and orbitofrontal region. These fiberes are embedded within the anterior limb of the internal capsule (*alic*) where fibers from various sources are arranged in a coarse topological order (Safadi et al., 2018).The *athr* fibers are also not intermingled within *alic* but form a circumscribed bundle in the most medial and ventral position (Fig. 15 c,d).

The *athr* fibers pass above the anterior commissure between the caudate and the accumbens nucleus to reach the pre- and orbitofrontal cortex. These anteriorly directed fibers are depicted in a paramedian section in Fig. 15 a. The sagittal section in Fig. 15 b shows the partially segregated fibers of AV and AM in the prereticular zone of the thalamus where *sm, st, fx, athr* and *ithp* converge. The frontal section (Fig. 15 c) presents the location of the *athr* in the medial partition of *alic*. Fig. 15 d shows the continuity with the frontal cortex.

3.4. Dorsal diencephalic conduction system

The stria medullaris (*sm*) and its relation with the stria medullaris bed (anteriorly) and the habenula (posteriorly) is clearly demarcated in the histological section as is the fasciculus retroflexus (Fig. 16a). Both components are are well outlined in the sagittal tractograms. Figs. 16b and c show the *sm* fibers well posterior to the anterior commissure distinguishing the stria medullaris bed from the BNST.

We were not able to follow the fasciculus retroflexus to its target areas, the Ip, ventral tegmental ncl. of Gudden or the raphe nuclei (Aizawa et al., 2011; Fig. 17).

3.5. Internal medullary lamina

The anterior portion of the internal medullary lamina (*iml*) forms a calix around the base of ANT (Fig. 18) and has intense fiber exchange with the ANT. Together with some midline nuclei it also projects to the limbic cortex (Robertson and Kaitz, 1981; Matsuoka, 1986; Vogt et al.,1987). The overall connections are very distributed and therefore it was not possible to separate any specific projection to the ANT from those related to the basal ganglia and caudally directed fibers. The intimate relation of the anterior *iml* with the ANT (Fig. 18) inevitably provokes co-activation by DBS stimulation of the ANT.

3.6. Nigrothalamic fibers

The efferent GABA-ergic fibers from the (posterior) substantia nigra pars reticulata (SNRp) reach the ANT alongside of the *mth* passing through the intralaminar formation lateral to the mediodorsal nucleus (Carpenter and Peter; 1972; Mai and Forutan, 2012). We were able to convincingly demonstrate this connection until the undersurface of the AV around the base of the entry zone of the mammillothalamic tract (Fig. 19). This location provides an extremely complex composition of diverse cellular and fibrous elements as indicated in Figure 18. It comprises VAmc where a sweet spot for positive outcome after DBS in epilepsy patients has been found (Majtanik et al., 2021).

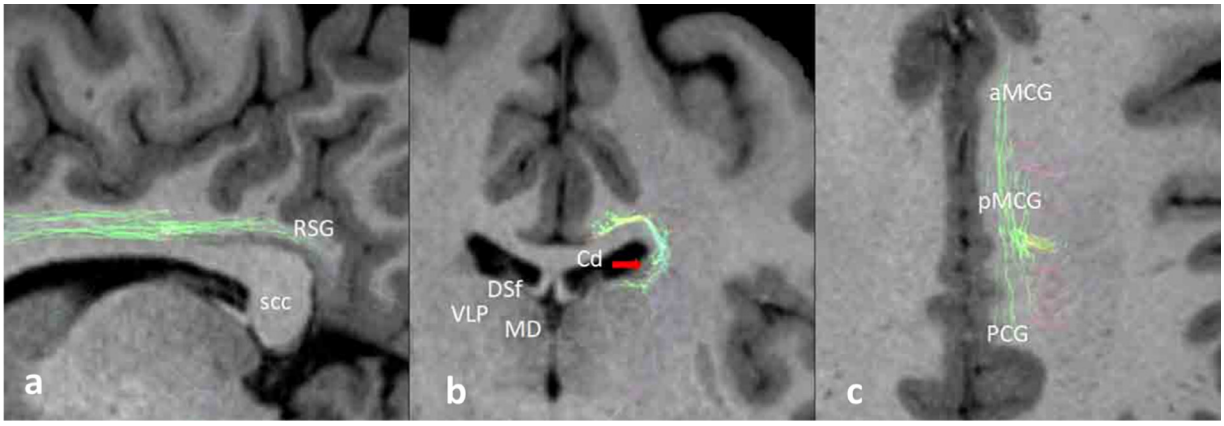

Fig. 11. The trajectory of the thalamocingulate fibers that leave the ANT region as part of the paramedian or limbic radiation displayed in T1 images. These ANT efferents turn around the ventral and lateral border of the caudate nucleus and extend within the basolateral division of the cingulate gyrus.

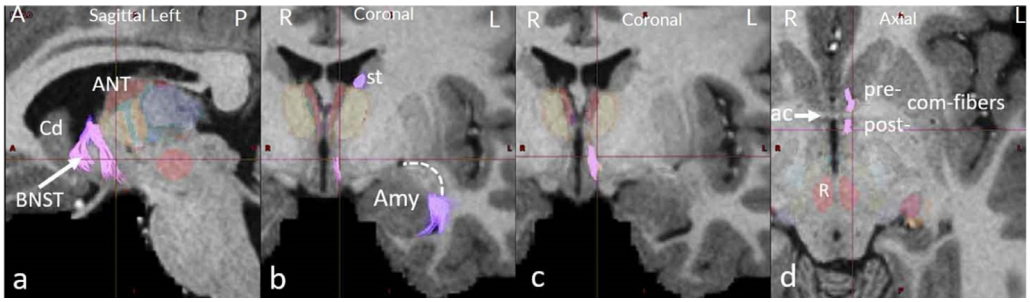

Fig. 12. Delineation of the stria terminalis, bed nucleus of the stria terminalis and associated fibers. The white broken line (b) indicates the course of *vap* fibers in more anterior section planes.

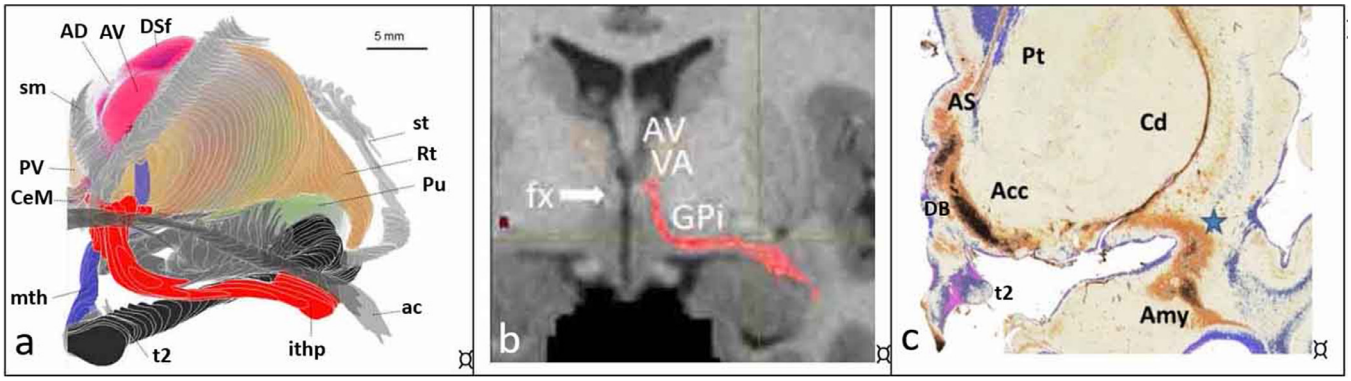

Fig. 13. Inferior thalamic peduncle (*ithp*) and ventral amygdalofugal pathway. (a) Anterior view on the reconstruction of the human thalamus and some related fibers. Highlighted are the three ANT nuclei (pink) surrounded by the stria medullaris (*sm*) and stria terminalis (*st*) and the inferior thalamic peduncle (*pthi*, red). The mammillothalamic tract is shown in blue. (b) Trajectory of the *ithp* as determined by DDT. (c) Cholinergic system (brown and black) in the basal forebrain area and the anterior temporal lobe (color enhanced frontal section immunostained for nerve growth factor receptor). The asterisk shows the approximate location of the "area tempestas".

3.7. The ANT fiber grid

Fig. 20 shows the reconstructed pathways as centroid fiber representation defined as a center of mass of all fibers belonging to a pathway. A single point on the centroid fibers is approximately the center of mass of the nearest points in the fibers of the pathway. The densest point in this 3-D grid locates near the ending of the mammillothalamic tract.

4. Discussion

The ANT represents a convergence zone with in- and output-relations of many regions which are associated with quite diverse functions. The detailed and anatomically valid reconstruction of the fiber pathways of the ANT region serves as basis for a connectivity profile of the ANT represented in the common ICBM/MNI 2009b space. Under the preposition that target and source areas of these pathways cover segregated territories in the ANT this knowledge may be used for the planning of DBS in epilepsy.

4.1. Microscopic information providing improved selectivity and specificity

High-resolution microscopic information was used for guiding the non-invasive *in-vivo* imaging. We applied dMRI-based tractography to derive at a structural description of the connectedness of brain regions

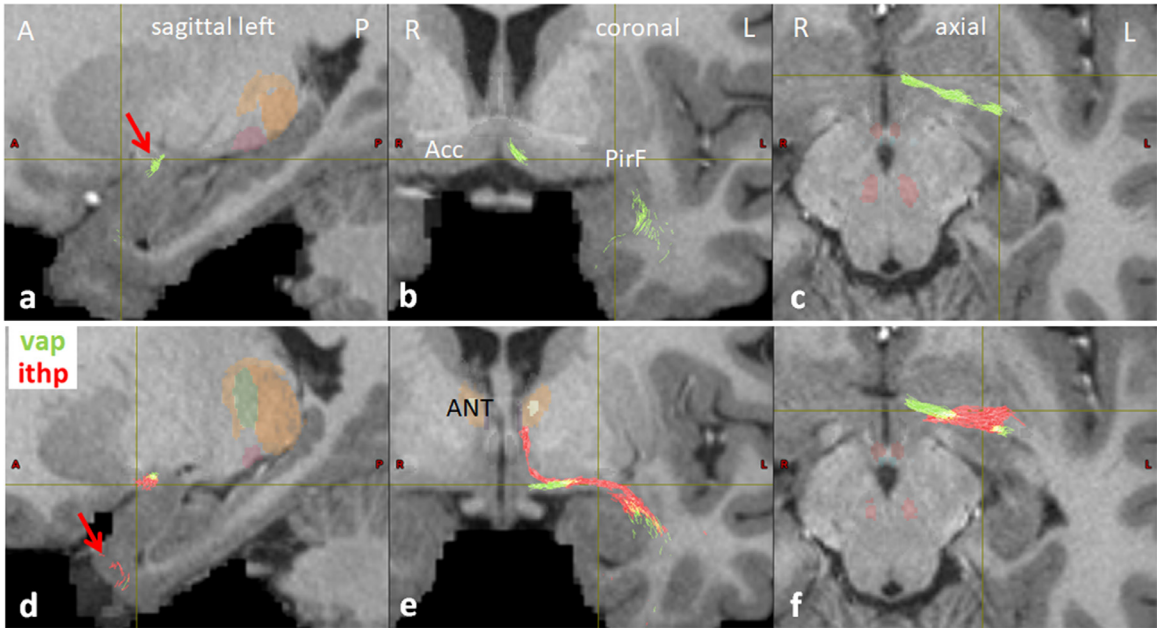

Fig. 14. Top row (a-c): The course of the ventral amygdalofugal pathway (*vap*, green). Lower row (d-f): Demonstration of the *vap* compared with the trajectory of the inferior thalamic peduncle (*ithp*, red) in a T1 scan. Arrow in a indicates the small extension of *vap*.

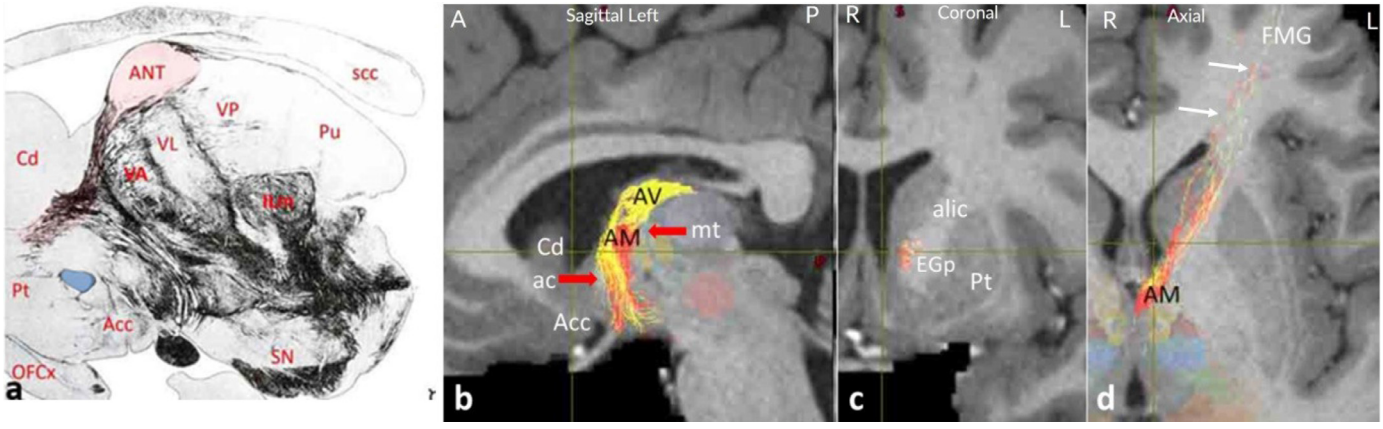

Fig. 15. Components of the orbitofrontal system. (a) Sagittal section highlighting the ANT with its fiber relation of the anterior thalamic radiation (*athr*, red); anterior commissure: blue. Drawing of a parasagittal fiber stained section; modified from Vogt and Vogt (1904). (b-d) Partial segregation of the *athr* projections from AV (yellow) and AM (red). Both fiber streams locate in the most medial portion of *alic*. Scattered fibers (white arrows) can be traced to the region of the middle frontal gyrus (FMG). (T1 scan).

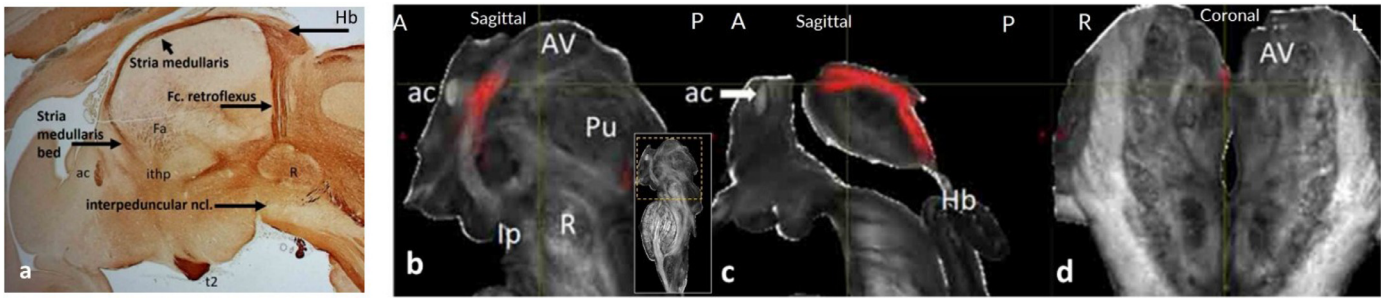

Fig. 16. Dorsal diencephalic conduction route. (a). The sagittal section (GAP-43 immunoreactivity) through the human thalamus depicts the stria medullaris thalami and the fasciculus retroflexus interrupted by the habenular nuclei. (b,c). The stria medullaris (red) in sagittal plane shows the close relation to AM. The coronal section (d) reveals sm at the caudomedial border of AV. Figs (b-d) show FA modality of the brainstem scan. The three canonical sections are cut perpendicular to the brainstem axis of Meynert and are displayed as a navigation box in the lower right corner of (b).

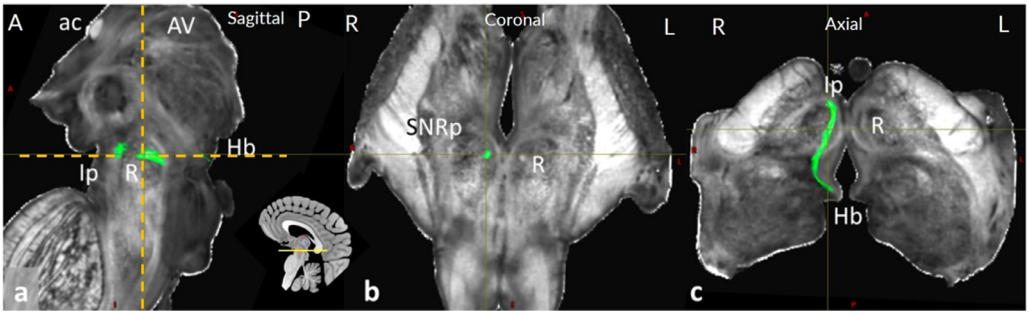

Fig. 17. The course of the fc. retroflexus between Hb and Ip (green)) shown on the FA brainstem sections rotated in such a manner that the axial section cut through the fasciculus. The rotation and the orientation of the brainstem is depicted with the locator image in the right low corner of (a). The navigation box shows the sagittal section of the rotated brainstem overlaid onto the MNI brain.

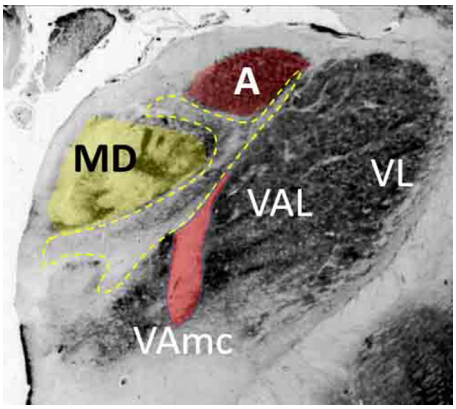

Fig. 18. Coronal section through the anterior third of the thalamus at 25 weeks of gestation. The three main divisions (anterior, A, medial, MD, and lateral, VAmc, VAL, VL) are separated by the intralaminar formation, outlined by the yellow stippling. The mth (red color) is surrounded by VAmc before it passes through iml to reach the ANT.

in-vivo (Johansen-Berg and Rushworth (2009). However, this methodology alone is an inherently limited approach that has variable degrees of selectivity and specificity and requires augmenting strategies to accurately describe the intricate anatomy and connectivity of the human brain (Schilling et al., 2019). This was achieved by a hybrid approach combining a histological (*in-vitro*) approach providing improved selectivity and specificity for the *in-vivo* tract tracing of anatomical connectivity.

Our Synthetic Pathway Reconstruction (SPR) process thus combined histological and tractographic data of the fiber bundles. It results in a pathway atlas that explicitly integrates the discriminated fiber bundle priors from histological (microscale) sections with the streamlines provided by probabilistic tractography. The pathways show a complex topography with very different spatial orientations and different fiber strength, a feature which we described as “fiber grid map” representation (Fig. 20). With this approach we aimed to discriminate and characterize those fiber bundles which are known to being related to the ANT on a microscopic scale. This ANT atlas represents a multi-layer template which embeds microscopic resolution of individual anatomy with the mesoscale resolution provided by in vivo imaging. The anatomical detail far exceeds the capabilities of any current tractography algorithm.

4.2. Limitations to define ANT subdivisions in the human brain

The analysis of the connectivity in humans is challenging because of the high variability of the ANT region, interindividual differences, age and disease related changes (Hughes et al., 2012; Akeret et al. 2021, Suppl. Fig. 5). Many structural features are still unknown in humans and principal differences exist between the human and non-human ANT. Information derives mainly from clinico-pathological findings and interpretation of experimental data obtained in animals. Therefore, when describing the anatomical and functional relationships of the human ANT and its associated pathways, we rely on relatively sketchy information.

As most information about the structure and connectivity of the human ANT derives from animal studies some major organizational differences shall be noticed: *First*, the topography and relative size of the ANT subnuclei differ between humans and subhuman species. This is particularly evident for the AD, which in humans undergoes a prominent reduction in volume (Hopf, Gihr and Kraus, 1967). *Second*, many tracts related to the ANT are well demarcated (*mth, sm, st, sz*) but their mode of termination in the ANT subnuclei in humans is unclear and often described in analogy with animal studies where the connectivity of most components is characterized by distinct and segregated pathways (Poletti and Creswell, 1977). *Third*, the methodology did not utilize the chemoarchitectonic properties to distinguish the source and target areas of projections in the ANT. *Lastly*, we neither did consider the role of interneurons which show fundamental interspecies differences (Letinic and Rakic, 2001; Mathiasen et al., 2020) nor the microenvironment by glial cells and ECM-components that contribute to the etiology of epilepsy (Devinsky et al.,·2013; see Patel et al., 2019). We have minimized the disadvantages by integrating results from additional cyto-, fiber- and chemoarchitectonic resources.

Are the tools appropriate to distinguish the fiber elements of the ANT region? dMRI-based tractography allows localization of white matter bundles *in-vivo* (Jbabdi and Johansen-Berg, 2011). In view of the many limitations that exist about the specificity and selectivity of the fiber systems, it is essential to use adequate methods for their characterization (Schilling et al., 2021). One accurate approach in the case of complex fiber configurations is the use of the fiber orientation density function (fODF) which estimates the directions of fiber distribution in each voxel. In this work we use the multi-tissue multi-shell constrained spherical deconvolution for the HCP and brainstem data, and multi-tissue single shell for the postmortem whole brain data (Tournier et al., 2004; Tournier et al. 2007; Jeurissen et al. 2014). These methods provide estimates of the fODF and a discrete number of crossing orientations in each voxel. The estimation of the crossings and the optimality of deconvolution methods are essential for tracking the white matter fibers (Behrens et al. 2007). As with all diffusion-weighted reconstructions, the generated fiber tracts only describe the diffusivity in the region of interest and it is assumed that this corresponds to what is or can be described as a real existing tract.

Several validation studies tested if and how accurate tractography can separate fiber bundles and follow them through white matter (Maier-Hein et al., 2017). Qualitative analyses have shown good agreement with histological tracing methods in the monkey

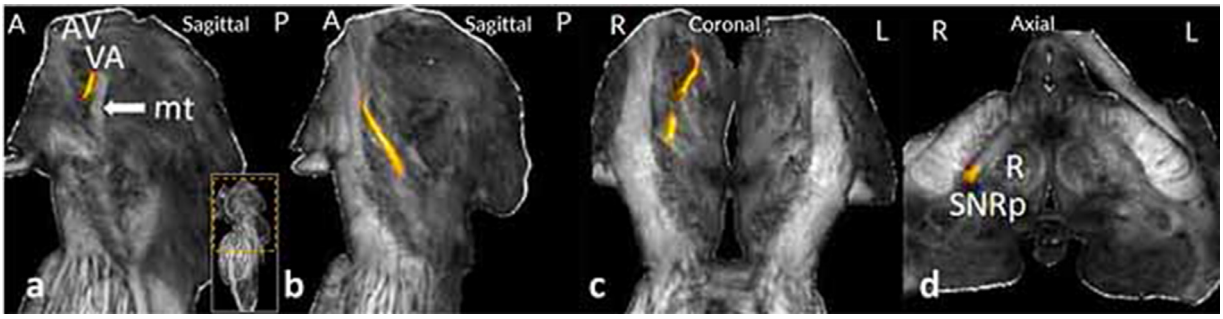

Fig. 19. Course of fibers between the posterior substantia nigra (SNRp) and AV (orange streamline), passing through the intralaminar formation and the magnocellular ventroanterior nucleus of the thalamus (VAmc). The FA modality of the brainstem is shown. The three canonical sections are cut perpendicular to the brainstem axis of Meynert and displayed as a navigation box in the lower right corner of (a).

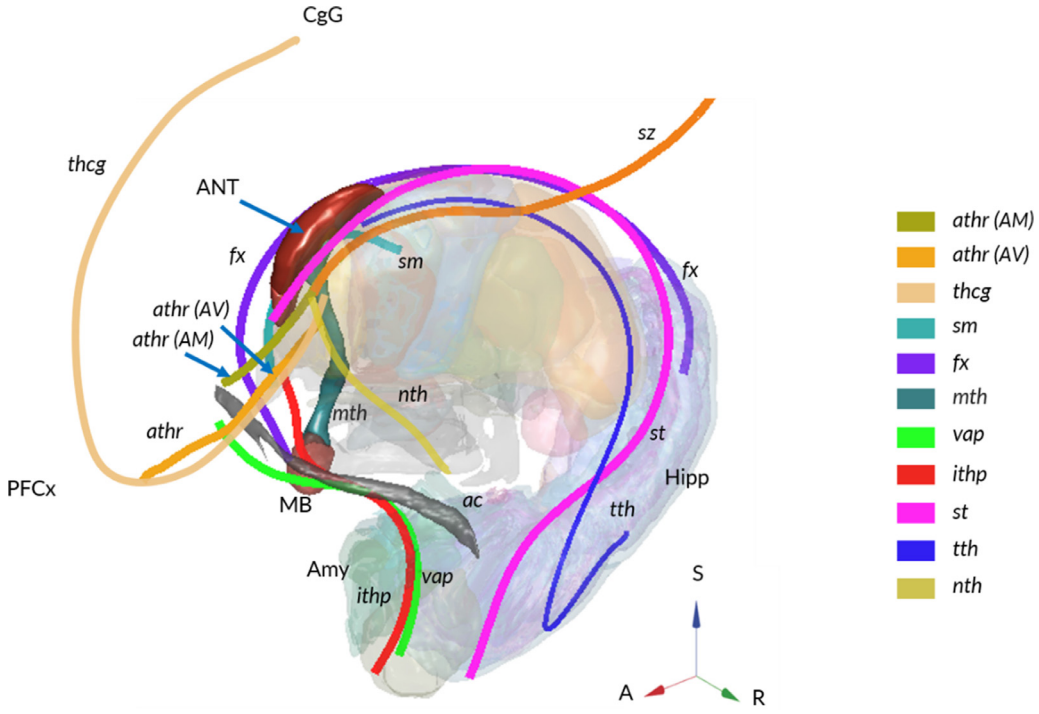

Fig. 20. The centroid representation of the final ANT fiber grid. Each reconstructed pathway is represented as a single centroid fiber embedded onto transparent 3D thalamus model with the ANT, mammillothalamic tract (mth) and mammillary body (MB) shown in solid colors. For orientation, the prefrontal cortex (PFCx), cingulate gyrus (CgG), amygdala (Amy) and hippocampus (Hip) are indicated. The orientation is indicated by the colored coordinate system arrays with anterior A, right R and superior S directions. For further abbreviations see list of abbreviations.

(Schmahmann et al. 2007) and in the human brain (Lawes et al., 2008). However, novel comparisons have also stressed the false positive connection problem in the fiber estimates (Dyrby et al., 2007; Dauguet et al., 2007). Further, it was shown that the probabilistic tractography is less sensitive to anisotropy and curvature and shows more sensitivity, but less specificity, than deterministic methods (Thomas et al., 2014). This results in a higher susceptibility to false positives which we account for with the anatomical fiber bundle priors. This higher specificity allows including the relevant fibers in the selected bundles. In our iteration procedure we optimize the corresponding parameters for inclusion of less pronounced fibers. The integration of the fiber priors defined from microscopic anatomy also reduces the seed bias.

To increase the selectivity of our reconstruction we used the anatomical fiber models (priors) to clean up the fiber bundles. In a first step all fibers were removed that did not correspond to the anatomical prior and in the second step the fiber bundles were inspected and revised by an anatomical expert.

4.3. Location and trajectory of each selected tract and the possible relevance for seizure mechanisms

4.3.1. Extended Papez circuit

Experimental and clinical studies have shown that disturbances within the extended Papez circuit are associated with the pathogenesis of epilepsy (Stypulkowski et al., 2014, Gross et al., 2021, Vonck et al., 2007). We clearly delineated in our analysis the “classical” fibers linking hippocampal regions, ANT and cingulate gyrus but we realized differences with respect to descriptions in animals.

ANT afferents: The *direct* input for the ANT was described to detach from the retrocommissural fornix and to turn around the inferior border of the foramen of Monroe to reach the ANT (Percheron, 2004). This direct projection to the thalamus is documented in monkey as a voluminous bundle (Poletti and Creswell, 1977) but has to our knowledge never convincingly mapped as a robust pathway to the ANT in humans. The physiological consequences of the activity of this proposed direct hippocampal pathway are not known.

The anatomic organization of the precommissural fornix fibers appears also to differ from the established concept where these are shown to separate from the fornix column as rather compact bundle directly above the anterior commissure (Poletti and Creswell, 1977). Quite differently, Fig. 7 shows the immunostained fibers leaving the column successively along the septum to reach the limbic forebrain area. Such fibers are depicted in Riley's atlas (Riley, 1960) (p. 454) but labelled as "fasciculus olfactorius septi" to indicate their olfactory connection. The distinction between the pre- and postcommissural fornix fibers is important because the target of the precommissural fibers in the medial septal area (and diagonal band complex) is the source of cholinergic, GABAergic and glutamatergic neurons, in part connected with GABAergic interneurons in the hippocampus. Disturbance of the adjustment or deregulation of the excitatory-inhibitory balance of synaptic transmission in the hippocampus has been associated with temporal lobe epilepsy (Bonansco and Fuenzalida, 2016). Both, the cholinergic and GABAergic projections, propagate theta waves in the hippocampus contributing to the coordination of neuronal activity. Several lines of evidence support the concept that the theta rhythm plays an important role in specific brain processes (Colom, 2006) and appears as part of a seizure-resistant functional state (Miller et al., 1994).

The *mth* is mapped as a coherent fiber bundle connected only with the AV entrance zone not contributing to the remaining ANT subnuclei. This circumscribed relation of *mth* to this subnucleus only, presents a challenging fact in the light that in non-human mammals the mammillothalamic tract has a characteristic and precise topographic allocation with all anterior nuclei (Christiansen et al., 2016, Sikes et al., 1977; Swanson and Cowan, 1977; Seki and Zyo; 1984; Shibata, 1992; Dillingham et al., 2015). This finding has elementary functional implications because in non-humans a segregated organization of projections and intranuclear domains is maintained throughout the extended Papez circuit including the brainstem relations. For example, a pathway related to the medial mammillary nucleus is regarded as a theta rhythm related component of the mnemonic and orientation system; a lateral circuitry matches the head direction pathway utilizing distinctive network components (Bubb et al., 2017). The role of subcomponents of the MB or the *mth* is challenging in the light that pathology of these structures has been related to mesial temporal lobe epilepsy without noticable involvement of the hippocampus (see Meys et al., 2022).

The relationship between the mammillary body and the tegmental nuclei by the mammillotegmental tract and the mammillary peduncle falls out of the direct connections of the anterior nuclei. This relation is, however, relevant with respect to the possible persistence of the segregated organization of the brainstem connections with the extended hippocampal system. The important source of fibers from the cingulate cortex to the ANT is part of the reciprocal cortical connection and described below.

ANT efferents: The thalamocingulate projections (*thcg*) from each of the ANT subnuclei terminate in partly overlapping sectors along the anterior-posterior extension of the basolateral cingulate gyrus (possibly in a medial-to-lateral topographic organization). Whereas the topographic correlation and spatial order in this connection was already described for the monkey by Yakovlev et al. (1960), it is noticeable that there still exists very limited knowledge about the precise organization in humans. Two alternative routes were described in animal studies (Bubb et al., 2020). One (*thcg-a)* is taken by fibers that emanate from the ANT at the anterior limb of the internal capsule (*alic*). These fibers then locate not in *alic* as described in recent DTI studies (Weininger et al., 2019) but assemble more medially. We found appreciable numbers of fibers that reach the anaterior cingulate gyrus, contrasting the very few fibers described by Armstrong (1990). The other trajectory (*thcg-p)* consists of fibers that leave the ANT in the stratum zonale and perforate the callosal fibers to reach the limbus of the hemisphere (the base of the telencephalic evagination). These fibers were verified by the analysis of sections from developing (Krieg, 1973) and pathological human brains following rather circumscribed lesions (Yakovlev and Locke, 1961) (Fig. 10). The description of a dichotomous organization is probably simplified because the ANT efferents appear to continuously leave the anterior thalamus and join the fan of the corona radiata.

The knowledge of the regional distribution and their laminar organization would be important because the thalamocingulate projection interacts with diverse neuronal populations representing many functionally related systems with different outputs (Beckmann et al., 2009; Shibata and Yukie, 2009; Vogt, 2009). The cingulum and, more general, the cortico-thalamo-cortical circuits have been described as being involved in the generation and propagation of a large number of seizures (Vonck et al., 2007). Experimental investigations have detected neurons that are prone to rapidly recruit epileptic cortical networks (Sorokin et al., 2017; Gobbo et al., 2021). Other studies documented the involvement of the cingulum in the generation and propagation of seizures possibly by disinhibition due to decreased GABA input of the thalamic projection neurons (Tomitaka et al. 2000; Kremer et al., 2003).

4.3.2. Extended amygdaloid system

The fibers included in this system (*st, vap* and *ithp*) are well outlined. This is contrasted with the challenging array of fibers and their intricate relations. The postcommissural *st* fibers occupy an area that includes the ventromedial hypothalamic nucleus, the premammillary nucleus and the lateral hypothalamic area. This latter connection is important in the context of stress-related events and may be responsible for epileptic seizures (Gunn and Baram, 2017).

The ventral amygdalofugal pathway (*vap*) and the inferior thalamic peduncle (*ithp*) share the subpallidal corridor as passage of fibers related to either the septal nuclei or the limbic thalamus, including the AM. The distant affiliation of *ithp* is apparently more widespread and connects with the anterior and medial temporal lobe and olfactory cortex. Both pathways pass along the piriform cortex, involving the "area tempestas" which has been related to epileptogenesis and seizure propagation (Vismer et al., 2015), and below the basal nucleus of Meynert. This latter nucleus has also described as an area that is involved in epileptogenesis (González et al., 2021). The *ithp* fibers then become rather compact and curve dorsally around the medial margin of the emerging pallidal fibers to enter the polar reticular thalamic nucleus (Ncl. fasciculosus) where the fibers fan out towards their destination in the MDmc and AM. MDmc has been reported as an effective target for DBS in specific epilepsies (Juhász et al., 1999; Bertram et al., 2001). It is worth mentioning, that in all areas and nuclei high levels of CART (cocaine- and amphetamine-regulated transcript) peptide are present. This molecule has been related to the pathophysiology of epilepsy (Keating et al., 2008).

4.3.3. Orbitofrontal system

The connection between the ANT nuclei and the orbitofrontal cortex was described since the early last century (Sachs, 1909; Clark and Boggon, 1933; Waller, 1933). The orbitofrontal system together with the extended amygdaloid system have been jointly described as the (efferent) conduction systems of the amygdalo-thalamo-orbitofrontal organization and compared to that of the hippocampal formation (Nauta, 1962). Both systems are engaged in some common fundamental mechanisms mediated by the medial forebrain bundle (*mfb*). This connection has raised great interest because of psychophysiological implications (Coenen et al., 2012).

The medial forebrain bundle (*mfb*) is a loosely textured, bidirectional, transhypothalamic fronto-midbrain pathway related with the orbitofrontal system. In the lateral preoptico-hypothalamic continuum (Nieuwenhuys et al.,1982) it is situated between the cerebral peduncle and the fornix and then runs longitudinally to the ventral tegmental area (VTA). A superolateral-branch of the *mfb* has been described as a component that reaches the wider ANT region (Zyo et al., 1963; Coenen et al., 2012). We could only show those elements of the *mfb* fibers that can be followed in myelin sections but were not able to demonstrate the relation of *mfb* fibers with the ANT group of nuclei.

4.3.4. Stria medullaris thalami (part of the dorsal diencephalic conduction system)

The course of the stria medullaris (*sm*) is well discriminated in our tractogram with its dorsomedial course along the thalamus to the habenula. The compact bundle provides no difficulty and has earlier been investigated using diffusion-weighted imaging by a probabilistic (Kochanski et al., 2016) and also by an anatomically guided approach (Roddy et al., 2018). Anteriorly, *sm* derives from the frontolimbic "bed" around and behind the anterior commissure, an area that partially merges with the territory of the stria terminalis fibers. At the level of paratenial nucleus, regarded as an interstitial nucleus of the *sm* (Kuhlenbeck, 1951) the fibers are directly adjacent the AD.

By its direct connection with the habenula and the habenulo-interpeduncular tract (fasciculus retroflexus) the *sm* influences the cholinergic and monoaminergic output of the limbic midbrain area. The habenula is also linked to the ventral tegmental ncl. of Gudden, VTA, raphe nuclei and superior colliculus (Aizawa, 2011). All these targets are components of a network that have been related to the pathophysiology of epilepsy at least in experimental studies: the tegmental nuclei close the loop with the mammillary nuclei (by the mammillotegmental tract and the mammillary peduncle); activation of the deep layers of the superior colliculus exerts anticonvulsant effects (Wicker et al., 2019); the midbrain raphe nuclei influence arousal and cardiorespiratory function that may be compromised during seizures (Zhan et al., 2016).

4.3.5. Internal medullary lamina

The anterior part of the internal medullary lamina (*iml*) shows complex relations with the ANT. The *iml* fibers are highly collateralized and it was therefore not possible to separate the components for the ANT from those related to the basal ganglia or cortex (Robertson and Kaitz, 1981; Matsuoka, 1986; Vogt et al., 1987). As *iml* fibers are apposing the undersurface of AV and penetrate AM they are influenced by the VAT during ANT stimulation. The excitability of this region might affect the cholinergic and orexinergic network and thus interfere with the sleep-wake state resulting in effects on seizure threshold (Saalmann, 2004, Ng; 2017, Voges et al., 2015).

4.3.6. Nigrothalamic fibers

The nigrothalamic fibers are described as a loosely arranged array of thin axons. This arrangement differs from our result where a rather compact bundle is revealed that passes through VAmc before it reaches AV around the base of the entry zone of the *mth*. VAmc receives major GABAergic input from the basal ganglia, more specifically from the posterior division of the substantia nigra pars reticulata. The VAmc area around the entry zone corresponds to the hot spot for good postoperative outcome reported by Schaper et al. (2020). Our own analysis of a large cohort of epilepsy patients (the MORE study) also revealed a statistical sweet spot for good postoperative outcome that was located around the base of the entry zone of *mth* at the AV-VAmc transition (Majtanik et al., 2021). Because one or two tip contacts of the lead are quite often positioned at the lower part of the ANT and adjacent VAmc/Ilm-region it should be considered relevant for the effects of DBS in intractable epilepsy.

The involvement of the fibers from the substantia nigra pars reticulata (SNR) in the seizure-controlling network is widely discussed (Velísková and Moshé, 2006). It must be tested whether the same group of neurons from the SNR also involves the caudal deep layers of the superior colliculus. Both projections have been implicated in the control of brain stem convulsive seizures.

4.3.7. Neuromodulatory pathways

Neuromodulatory pathways are specified by their neurotransmitter or -peptide content. For understanding network activity and the modulation of cellular operation it is mandatory to describe their presence in the ANT and associated networks. They are difficult to demonstrate because of the much dispersed arrangement, extensive branching pattern and wide terminal fields.

The ANT receives afferents from a remarkable number of neurotransmitter systems. We mentioned trajectories that included cholinergic (Fig. 12) and dopamin- and GABAergic axons. The ANT has been described to receive the highest innervation density of cholinergic afferents to the diencephalon with predominance of the AD. They apparently do not originate from the NBM but from the pontine tegmental and the laterodorsal tegmental nuclei (Heckers et al., 1992). Like their action on sensory relay nuclei the cholinergic afferents may enhance the spontaneous and evoked activity in the ANT, affect the state of vigilance and may change the excitation-inhibition balance in circuit level function (Wang et al., 2021). Perturbations of DA neurotransmission have been related to behavioral abnormalities and may be directly involved in seizure facilitation in epilepsy (Bouilleret et al., 2008; Galovic and Koepp, 2016).

Adrenergic and noradrenergic afferents from the brainstem enter the anterior thalamus through the zona incerta and reticular nucleus and reach the ANT by the dorsal noradrenergic bundle (Lindvall and Björklund, 1983). Recent immunohistochemical analysis found heterogeneous distribution of DA-transporter-ir axons within the anterior nuclei (with moderate to dense immunolabeling in the AM and AV and very weak to poor immunolabeling in the AD and Dsf). A prominent density of histaminergic fibers was observed in AD.

The human ANT harbors up to 40% GABA-ergic interneurons (IN). They derive from the primate-specific-telencephalo-diencephalic migratory stream called corpus gangliothalamicum which is of relevance for the interpretation of animal studies with respect to human circumstances. The IN can be classified based on the expression of several neuropeptides and calcium-binding proteins. GABA-B (determined by GABA-B mRNA expression) that may regulate slow oscillations of thalamocortical neurons has been found in monkey AV with the highest level of the dorsal thalamus.

4.4. The relevance of the representation of the fiber pathways for the analysis of DBS outcomes

The final output of our synthetic reconstruction method is a unitary representation of the pathways in the MNI space (ICBM/MNI_2009b_symmetric) that is applicable for complex pathway activation analyses (Lujan et al., 2013; Hartmann et al., 2015). The ANT fiber grid map (Fig. 20) enables to identify axonal fiber bundles surrounding an individual electrode that are critical for optimal benefit and helps to better isolate the confounding factors.

In a theoretical analysis we studied the extent of pathway activations by the VAT of an active electrode (paper in publication). The positions of the contact varied in a dense grid (0.2 mm spacing) across the ANT region. We found that the activation pattern of fibers depends on the location and amplitude of the stimulation. Different positions showed distinct fiber activation patterns that modulate different seizure regulatory networks.

Optimal therapeutic results are associated with the activation of distinct and stable fiber pathways and cortical areas have been proven by pathway activation analysis of DBS in obsessive-compulsive disorder patients (Hartmann et al., 2016). In case of epilepsy, this association between the activated pathways and areas is not stationary but depends on the type of the epilepsy and the location of the epileptogenic zone. Additionally, the connectomes of the epileptic patients show complex alternations relative to the healthy population (Kreilkamp et al., 2021). We therefore propose to use the ANT fiber map with the individual patient dMRI in order to create a patient specific estimate of the networks that may be adjustably modulated by the ANT-DBS stimulation. This approach offers the possibility to modulate different domains of the network with respect to functional properties ascribed to subcomponents. This makes it possible to selectively manipulate the activation strength

of different networks, e.g., limbic vs. frontal. This selective modulation - derived from of the ANT fiber map - may potentially support the planning procedures. The combination of the quantification of ANT network activation ability with patient specific connectome of the epileptogenic zone (Jirsa et al., 2017; Proix et al., 2018) may significantly improve the identification of an optimal target location. Such detailed analysis is beyond the scope of this anatomical work but the focus of our future research.

We believe that the present work has significant impact on clinical practice both in neurosurgical implanting techniques as well as post-operative stimulation programming. In movement disorders like Parkinson's disease and essential tremor, targeting of specific white matter tracts rather than grey matter nuclei (Coenen et al., 2014; Avecillas-Chasin et al, 2019) is being implemented to clinical use in increasing manner. Analogically, the role of *mth* input to ANT was acknowledged early and targeting of *mth* has indeed been suggested as an alternative to ANT nucleus stimulation (Koeppen et al., 2019; Schaper et al., 2020). Our work combines detailed histological information and connectome -based fiber tract information and demonstrates the plethora of fiber tracts connected to ANT. We believe that this serves as a fundamental basis to individually tailored targeting of specific seizure spread pathways in epilepsy or potentially other limbic system circuitpathies. Importantly, the technology today enables current targeting via segmented leads to more specific substructures as well as sensing of neural signals in target area. Without full understanding of the complexity of 3D white matter networks these sophisticated capabilities may be of limited value.

In summary, this study provides the first anatomically realistic pathway map of the ANT region with the synthetic reconstruction method incorporating human histological and structural MRI data. We propose that this map can be used for detailed fiber-based analysis of the outcomes of the DBS studies and potentially for visualization during the neurosurgical planning procedures.

In future work, resting state functional magnetic resonance imaging (fMRI) or individual Diffusion Weighted magnetic resonance Imaging (DWI) on mesoscopic scales combined with electrophysiological analysis will help to identify (short range and long range) network idiosyncrasies in the different epileptic phenotypes based on a newly described fiber anatomical network. This work here might then serve as the anatomical template for such studies. The application of the here defined relations between individual ANT region fiber maps and their conjunction to specific epilepsy phenotypes (which are not the focus of this work) might in the future improve surgical electrode placement. If successful, this information might help to improve the predictability of the ANT-DBS stimulation outcomes.

Data availability

Data were provided by the Human Connectome Project (HCP); the Washington University, University of Minnesota, and Oxford University Consortium (Principal Investigators David Van Essen and Kamil Ugurbil; Grant No. 1U54MH091657) funded by 16 NIH institutes and centers that support the NIH Blueprint for Neuroscience Research; and the McDonnell Center for Systems Neuroscience at Washington University.

The research data associated with this work are not openly accessible but are available from the corresponding author upon reasonable request. In case that the community has additional or other interpretations of the relevant fiber sets we are willing to discuss and eventually revise the information in our 3D fiber map.

Declaration of Competing Interest

J.K.M is CEO of MRX-Brain GmbH, M.M. is data analyst and AI developer for MRX-Brain GmbH. M.M. F.G., K.L., J.K.M. have business relationships with Medtronics, which are makers of DBS devices, but none is related to the current work. V.A.C., has business relations with Medtronic, Boston Scientific and is advisor for Ceregate (Hamburg), Cortec (Freiburg) and InBrain (Spain). None of theses activities are related to the current work.

Credit authorship contribution statement

Milan Majtanik: Conceptualization, Methodology, Writing – original draft, Formal analysis, Software. **Frans Gielen:** Conceptualization, Methodology, Writing – original draft, Writing – review & editing. **Volker Arnd Coenen:** Conceptualization, Methodology, Writing – original draft, Writing – review & editing. **Kai Lehtimäki:** Writing – original draft, Writing – review & editing. **Jürgen Konrad Mai:** Conceptualization, Methodology, Writing – original draft, Writing – review & editing, Supervision.

Acknowledgment

In the preparation of this work we used data obtained from the MGH-USC Human Connectome Project (HCP) database (https://ida.loni.usc.edu/login.jsp); from Prof. Dr. Marc Tittgemeyer, MPI Cologne; Translational Neurocircuitry Group; from Prof. Alard Roebroek, Faculty of Psychology and Neuroscience, Computational Brain Connectivity lab (CBClab) EV Maastricht.

Supplementary materials

Supplementary material associated with this article can be found, in the online version, at doi:10.1016/j.neuroimage.2022.119551.

References

Adil, S.M., Calabrese, E., Charalambous, L.T., Cook, J.J., Rahimpour, S., Atik, A.F., Cofer, G.P., Parente, B.A., Johnson, G.A., Lad, S.P., White, L.E., 2021. A high-resolution interactive atlas of the human brainstem using magnetic resonance imaging. NeuroImage 237, 118135. doi:10.1016/j.neuroimage.2021.118135, Epub, May 2. PMID: 33951517; PMCID: PMC8480283.

Aggleton, J.P., O'Mara, S.M., Vann, S.D., Wright, N.F., Tsanov, M., Erichsen, J.T., 2010. Hippocampal-anterior thalamic pathways for memory: uncovering a network of direct and indirect actions. Eur. J. Neurosci. 31, 2292–2307. doi:10.1111/j.1460-9568.2010.07251.x.

Akeret, K., van Niftrik, C.H.B., Sebök, M., Muscas, G., Visser, T., Staartjes, V.E., Marinoni, F., Serra, C., Regli, L., Krayenbühl, N., Piccirelli, M., Fierstra, J., 2021. Topographic volume-standardization atlas of the human brain. Brain Struct. Funct. 226, 1699–1711. doi:10.1007/s00429-021-02280-1.

Aizawa, H., Amo, R., Okamoto, H., 2011. Phylogeny and ontogeny of the habenular structure. Front. Neurosci. 5, 138. doi:10.3389/fnins.2011.00138, PMID: 22203792; PMCID: PMC3244072.

Alheid, G.F., Heimer, L., Switzer, R.C., 1990. The basal ganglia. In: Paxinos, G. (Ed.), The Human Nervous System. Academic Press, San Diego, pp. 483–582.

Alheid, G.F., 2003. Extended amygdala and basal forebrain. Ann. New York Acad. Sci. 985, 185–205. doi:10.1111/j.1749-6632.2003.tb07082.x.

Armstrong, E., 1990. Limbic thalamus: anterior and mediodorsal nuclei. In: Paxinos, G. (Ed.), The Human Nervous System. Academic Press, New YorkSan Diego, pp. 469–481.

Ashwell, K.W., Mai, J.K., 2012. Fetal development of the central nervous system. In: Mai, J.K., Paxinos, G. (Eds.), The Human Nervous System. Academic Press/Elsevier, San Diego, pp. 31–79.

Avecillas-Chasin, J.M., Hurwitz, T.A., Bogod, N.M., Honey, C.R., 2019. An analysis of clinical outcome and tractography following bilateral anterior capsulotomy for depression. Stereotact. Funct. Neurosurg. 97 (5-6), 369–380. doi:10.1159/000505077, Epub 2019 Dec 20. PMID: 31865344.

Bartolomei, F., Lagarde, S., Wendling, F., McGonigal, A., Jirsa, V., Guye, M., Bénar, C., 2017. Defining epileptogenic networks: contribution of SEEG and signal analysis. Epilepsia 58, 1131–1147. doi:10.1111/epi.13791, Epub 2017 May 20. PMID: 28543030.

Beckmann, M., Johansen-Berg, H., Rushworth, M., 2009. Connectivity-based parcellation of human cingulate cortex and its relation to functional specialization. J. Neurosci. 29 (4), 1175–1190. doi:10.1523/JNEUROSCI.3328-08.2009.

Behrens, T.E., Berg, H.J., Jbabdi, S., Rushworth, M.F., Woolrich, M.W., 2007. Probabilistic diffusion tractography with multiple fibre orientations: what can we gain? Neuroimage 34 (1), 144–155. doi:10.1016/j.neuroimage.2006.09.018, 2007 Jan 1Epub 2006 Oct 27. PMID: 17070705; PMCID: PMC7116582.

Bernhardt, B.C., Fadaie, F., Liu, M., Caldairou, B., Gu, S., Jefferies, E., Smallwood, J., Bassett, D.S., Bernasconi, A., Bernasconi, N., 2019. Temporal lobe epilepsy: hippocampal pathology modulates connectome topology and controllability. Neurology 92 (19), e2209–e2220. doi:10.1212/WNL.0000000000007447, 7Epub 2019 Apr 19. PMID: 31004070; PMCID: PMC6537128.

Bernstein, HG, Krause, S, Krell, D, Dobrowolny, H, Wolter, M, Stauch, R, Ranft, K, Danos, P, Jirikowski, GF, Bogerts, B., 2007. Strongly reduced number of parvalbumin-immunoreactive projection neurons in the mammillary bodies in schizophrenia: further evidence for limbic neuropathology. Ann. N Y Acad. Sci. 1096, 120–127. doi:10.1196/annals.1397.077, 2007 JanPMID: 17405923.

Bertram, EH, Mangan, PS, Zhang, D, Scott, CA, Williamson, JM., 2001. The midline thalamus: alterations and a potential role in limbic epilepsy. Epilepsia 42, 967–978. doi:10.1046/j.1528-1157.2001.042008967.x, PMID: 11554881.

Bettus, G, Guedj, E, Joyeux, F, Confort-Gouny, S, Soulier, E, Laguitton, V, Cozzone, PJ, Chauvel, P, Ranjeva, JP, Bartolomei, F, Guye, M., 2009. Decreased basal fMRI functional connectivity in epileptogenic networks and contralateral compensatory mechanisms. Human Brain Mapping 30 (5), 1580–1591. doi:10.1002/hbm.20625.

Bettus, G, Wendling, F, Guye, M, Valton, L, Régis, J, Chauvel, P, Bartolomei, F., 2008. Enhanced EEG functional connectivity in mesial temporal lobe epilepsy. Epilepsy Res. 81, 58–68. doi:10.1016/j.eplepsyres.2008.04.020, Epub 2008 Jun 10. PMID: 18547787.

Bonansco, C, Fuenzalida, M., 2016. Plasticity of hippocampal excitatory-inhibitory balance: missing the synaptic control in the pileptic brain. Neural Plasticity, 8607038 doi:10.1155/2016/8607038, Article ID.

Bouilleret, V, Semah, F, Chassou, F, Mantzaridez, M, Biraben, A, Trebossen, R, Ribeiro, M-J., 2008. Basal ganglia involvement in temporal lobe epilepsy. A functional and morphologic study. Neurology 70 (3), 177–184. doi:10.1212/01.wnl.0000297514.47695.48.

Bubb, EJ, Kinnavane, L, Aggleton, JP., 2017. Hippocampal-diencephalic-cingulate networks for memory and emotion: An anatomical guide. Brain Neurosci. Adv. 1 (1), 2398212817723443. doi:10.1177/2398212817723443, Aug 4.

Bubb, EJ, Nelson, AJD, Cozens, TC, Aggleton, JP., 2020. Organisation of cingulum bundle fibres connecting the anterior thalamic nuclei with the rodent anterior cingulate and retrosplenial cortices. Brain Neurosci. Adv. 4 2020 Sep 29398212820957160PMID: 32964131; PMCID: PMC7488606.

Calabrese, E., Hickey, P., Hulette, C., Zhang, J., Parente, B., Lad, S.P., Johnson, G.A., 2015. Postmortem diffusion MRI of the human brainstem and thalamus for deep brain stimulator electrode localization. Hum Brain Mapp. 36 (8), 3167–3178. doi:10.1002/hbm.22836, Epub 2015 Jun 3. PMID: 26043869; PMCID: PMC4652933.

Carpenter, MB, Peter, P., 1972. Nigrostriatal and nigrothalamic fibers in the rhesus monkey. J. Comp. Neurol. 144 (1), 93–115. doi:10.1002/cne.901440105, PMID: 4623850.

Cataldi, M., Avoli, M, de Villers-Sidani, E., 2013. Resting state networks in temporal lobe epilepsy. Epilepsia 54 (12), 2048–2059. doi:10.1111/epi.12400.

Chen, B, Xu, C, Wang, Y, Lin, W, Wang, Y, Chen, L, Cheng, H, Xu, L, Hu, T, Zhao, J, Dong, P, Guo, Y, Zhang, S, Wang, S, Zhou, Y, Hu, W, Duan, S, Chen, Z, 2020. A disinhibitory nigra-parafascicular pathway amplifies seizure in temporal lobe epilepsy. Nat. Commun. 11 (1), 923. doi:10.1038/s41467-020-14648-8, PMID: 32066723; PMCID: PMC7026152.

Christiansen, K, Metzler-Baddeley, C, Parker, GD, Muhlert, N, Jones, DK, Aggleton, JP, Vann, SD., 2016. Topographic separation of fornical fibers associated with the anterior and posterior hippocampus in the human brain: An MRI-diffusion study. Brain Behav. 7 (1), e00604. doi:10.1002/brb3.604, 2016 Nov 22PMID: 28127522; PMCID: PMC5256187.

Clark, WE, Boggon, RH., 1933. On the Connections of the anterior nucleus of the thalamus. J. Anat. 67 (2), 215–226 1933 JanPt9. PMID: 17104418; PMCID: PMC1249340.

Coenen, VA, Panksepp, J, Hurwitz, TA, Urbach, H, Mädler, B., 2012. Human medial forebrain bundle (MFB) and anterior thalamic radiation (ATR): imaging of two major subcortical pathways and the dynamic balance of opposite affects in understanding depression. J. Neuropsychiatry Clin. Neurosci. 24 (2), 223–236. doi:10.1176/appi.neuropsych.11080180, PMID: 22772671.

Coenen, VA, Reisert, M., 2021. DTI for brain targeting: diffusion weighted imaging fiber tractography—assisted deep brain stimulation. Int. Rev. Neurobiol. 47–67. doi:10.1016/bs.irn.2021.07.001.

Coenen, VA, Allert, N, Paus, S, Kronenbürger, M, Urbach, H, Mädler, B., 2014. Modulation of the cerebello-thalamo-cortical network in thalamic deep brain stimulation for tremor: a diffusion tensor imaging study. Neurosurgery 75 (6), 657–669. doi:10.1227/NEU.0000000000000540, discussion 669-70.

Coizet, V, Heilbronner, SR, Carcenac, C, Mailly, P, Lehman, JF, Savasta, M, David, O, Deniau, JM, Groenewegen, HJ, Haber, SN., 2017. Organization of the anterior limb of the internal capsule in the rat. J. Neurosci. 37 (10), 2539–2554. doi:10.1523/JNEUROSCI.3304-16.2017.

Colom, LV., 2006. Septal networks: relevance to theta rhythm, epilepsy and Alzheimer's disease. J. Neurochem. 96 (3), 609–623. doi:10.1111/j.1471-4159.2005.03630.x, 2006Epub 2006 Jan 9. PMID: 16405497.

Dauguet, J, Peled, S, Berezovskii, V, Delzescaux, T, Warfield, SK, Born, R, Westin, CF., 2007. Comparison of fiber tracts derived from in-vivo DTI tractography with 3D histological neural tract tracer reconstruction on a macaque brain. Neuroimage 37 (2), 530–538. doi:10.1016/j.neuroimage.2007.04.067, Epub 2007 May 24. PMID: 17604650.

Deppe, M, Kellinghaus, C, Duning, T, Möddel, G, Mohammadi, S, Deppe, K, Schiffbauer, H, Kugel, H, Keller, SS, Ringelstein, EB, Knecht, S., 2008. Nerve fiber impairment of anterior thalamocortical circuitry in juvenile myoclonic epilepsy. Neurology 71 (24), 1981–1985. doi:10.1212/01.wnl.0000336969.98241.17, 9PMID: 19064879.

Devinsky, O, Vezzani, A, Najjar, S, De Lanerolle, NC, Rogawski, MA., 2013. Glia and epilepsy: excitability and inflammation. Trends Neurosci. 36 (3), 174–184. doi:10.1016/j.tins.2012.11.008, Epub 2013 Jan 5. PMID: 23298414.

Dillingham, CM, Frizzati, A, Nelson, AJ, Vann, SD., 2015. How do mammillary body inputs contribute to anterior thalamic function? Neurosci. Biobehav. Rev. 54, 108–119. doi:10.1016/j.neubiorev.2014.07.025.

Domesick, VB., 1970. The fasciculus cinguli in the rat. Brain Res. 20 (1), 19–32. doi:10.1016/0006-8993(70)90150-2, 20PMID: 5444766.

Dyrby, TB, Søgaard, LV, Parker, GJ, Alexander, DC, Lind, NM, Baaré, WF, Hay-Schmidt, A, Eriksen, N, Pakkenberg, B, Paulson, OB, Jelsing, J., 2007. Validation of in vitro probabilistic tractography. Neuroimage 37 (4), 1267–1277. doi:10.1016/j.neuroimage.2007.06.022, 2007 Oct 1Epub 2007 Jul 10. PMID: 17706434.

Fisher, R, Salanova, V, Witt, T, Worth, R, Henry, T, Gross, R, Oommen, K, Osorio, I, Nazzaro, J, Labar, D, Kaplitt, M, Sperling, M, Sandok, E, Neal, J, Handforth, A., Stern, J, DeSalles, A, Chung, S, Shetter, A, Bergen, DSANTE Study Group, 2010. Electrical stimulation of the anterior nucleus of thalamus for treatment of refractory epilepsy. Epilepsia 51 (5), 899–908. doi:10.1111/j.1528-1167.2010.02536.x.

Galovic, M, Koepp, M., 2016. Advances of molecular imaging in epilepsy. Curr. Neurol. neurosci. Reports 16 (6), 58. doi:10.1007/s11910-016-0660-7.

Gimenes, C, Malheiros, JM, Battapady, H, Tannus, A, Hamani, C, Covolan, L., 2019. The neural response to deep brain stimulation of the anterior nucleus of the thalamus: a MEMRI and c-Fos study. Brain Res. Bull. 147, 133–139. doi:10.1016/j.brainresbull.2019.01.011, Epub 2019 Jan 15. PMID: 30658130.

Glasser, MF, Sotiropoulos, SN, Wilson, JA, Coalson, TS, Fischl, B, Andersson, JL, Xu, J, Jbabdi, S, Webster, M, Polimeni, JR, Van Essen, DC, Jenkinson, M, 2013. The minimal preprocessing pipelines for the Human Connectome Project. Neuroimage 80, 105–124. doi:10.1016/j.neuroimage.2013.04.127, Epub 2013 May 11. PMID: 23668970; PMCID: PMC3720813.

Gobbo, D, Scheller, A, Kirchhoff, F., 2021. From physiology to pathology of cortico-thalamo-cortical oscillations: astroglia as a target for further research. Front. Neurol. 12, 661408. doi:10.3389/fneur.2021.661408, PMID: 34177766; PMCID: PMC8219957.

González, HFJ, Narasimhan, S, Johnson, GW, Wills, KE, Haas, KF, Konrad, PE, Chang, C, Morgan, VL, Rubinov, M, Englot, DJ., 2021. Role of the nucleus basalis as a key network node in temporal lobe epilepsy. Neurology 96 (9), e1334–e1346. doi:10.1212/WNL.0000000000011523, 2021 Mar 2Epub 2021 Jan 13. PMID: 33441453; PMCID: PMC8055321.

Gonzalo-Ruiz, A, Sanz, JM, Lieberman, AR., 1996. Immunohistochemical studies of localization and co-localization of glutamate, aspartate and GABA in the anterior thalamic nuclei, retrosplenial granular cortex, thalamic reticular nucleus and mammillary nuclei of the rat. J. Chem. Neuroanat. 12 (2), 77–84. doi:10.1016/s0891-0618(96)00180-9, 1996 Dec.

Grodd, W, Kumar, VJ, Schüz, A, Lindig, T, Scheffler, K., 2020. The anterior and medial thalamic nuclei and the human limbic system: tracing the structural connectivity using diffusion-weighted imaging. Sci. Rep. 10, 10957. doi:10.1038/s41598-020-67770-4.

Gross, RE, Fisher, RS, Sperling, MR, Giftakis, JEStypulkowski PH on behalf of the SANTÉ Study Group, 2021. Analysis of deep brain stimulation lead targeting in the stimulation of anterior nucleus of the thalamus for epilepsy clinical trial. Neurosurgery 89 (3), 406–412. doi:10.1093/neuros/nyab186, PMID: 34161589; PMCID: PMC8374968.

Guo, W, Koo, BB, Kim, JH, Bhadelia, RA, Seo, DW, Hong, SB, Joo, EY, Lee, S, Lee, JI, Cho, KR, Shon, YM., 2020. Defining the optimal target for anterior thalamic deep brain stimulation in patients with drug-refractory epilepsy. J. Neurosurg. 134 (3), 1054–1063. doi:10.3171/2020.2.JNS193226, PMID: 32384279.

Gunn, BG, Baram, TZ., 2017. Stress and seizures: space, time and hippocampal circuits. Trends Neurosci. 40 (11), 667–679. doi:10.1016/j.tins.2017.08.004.

Hartmann, CJ, Chaturvedi, A, Lujan, JL., 2015. Quantitative analysis of axonal fiber activation evoked by deep brain stimulation via activation density heat maps. Front. Neurosci. 9, 28. doi:10.3389/fnins.2015.00028, PMID: 25713510; PMCID: PMC4322637.

Hartmann, CJ, Lujan, JL, Chaturvedi, A, Goodman, WK, Okun, MS, McIntyre, CC, Haq, IU., 2016. Tractography activation patterns in dorsolateral prefrontal cortex suggest better clinical responses in OCD DBS. Front. Neurosci. 9, 519. doi:10.3389/fnins.2015.00519, PMID: 26834544; PMCID: PMC4717315.

Heckers, S, Geula, C, Mesulam, MM., 1992. Cholinergic innervation of the human thalamus: dual origin and differential nuclear distribution. J. Comp. Neurol. 325 (1), 68–82. doi:10.1002/cne.903250107, PMID: 1282919.

Hopf, A, Gihr, M, Kraus, C., 1967. Vergleichende Architektonik des Primatenthalamus. In: Progress in Primatology. G. Fischer, Stuttgart, pp. 120–127.

Hu, B, Wang, Z, Xu, M, Zhu, L, Wang, D., 2021. The therapeutic mechanism of epilepsy seizures in different target areas: Research on a theoretical model. Technol. Health Care 29 (S1), 455–461. doi:10.3233/THC-218043.

Hughes, EJ, Bond, J, Svrckova, P, Makropoulos, A, Ball, G, Sharp, DJ, Edwards, AD, Hajnal, JV, Counsell, SJ., 2012. Regional changes in thalamic shape and volume with increasing age. Neuroimage 63 (3), 1134–1142. doi:10.1016/j.neuroimage.2012.07.043, Epub 2012 Jul 27. PMID: 22846656; PMCID: PMC3507623.

Järvenpää, S, Lehtimäki, K, Rainesalo, S, Möttönen, T, Peltola, J., 2020. Improving the effectiveness of ANT-DBS therapy for epilepsy with optimal current targeting. Epilepsia Open 5 (3), 406–417. doi:10.1002/epi4.12407, PMID: 32913949; PMCID: PMC7469781.

Jbabdi, S, Johansen-Berg, H., 2011. Tractography: where do we go from here? Brain Connect. 1 (3), 169–183. doi:10.1089/brain.2011.0033, Epub 2011 Aug 30. PMID: 22433046; PMCID: PMC3677805.

Jeurissen, B, Tournier, JD, Dhollander, T, Connelly, A, Sijbers, J., 2014. Multi-tissue constrained spherical deconvolution for improved analysis of multi-shell diffusion MRI data. Neuroimage 103, 411–426. doi:10.1016/j.neuroimage.2014.07.061, 2014 DecEpub 2014 Aug 7. PMID: 25109526.

Jirsa, VK, Proix, T, Perdikis, D, Woodman, MM, Wang, H, Gonzalez-Martinez, J, Bernard, C, Bénar, C, Guye, M, Chauvel, P, Bartolomei, F., 2017. The Virtual Epilep-

tic Patient: Individualized whole-brain models of epilepsy spread. Neuroimage 145 (Pt B), 377–388. doi:10.1016/j.neuroimage.2016.04.049, Epub 2016 Jul 28. PMID: 27477535.

Johansen-Berg, H, Rushworth, MF., 2009. Using diffusion imaging to study human connectional anatomy. Annu. Rev. Neurosci. 32, 75–94. doi:10.1146/annurev.neuro.051508.135735, PMID: 19400718.

Johnston, JB, 1923. Further contributions to the study of the evolution of the fore-brain. J. Comp. Neurol. 35, 371–482. doi:10.1002/cne.900350502.

Jones, EG, 1998. The thalamus of primates. In: Bloom, F.E., Björklund, A., Hökfelt, T. (Eds.), Handbook of Chemical Neuroanatomy, Vol. 14, The Primate Nervous System, Part II. Elsevier, Amsterdam, pp. 1–298. doi:10.1016/S0924-8196(98)80003-1.

Juhász, C, Nagy, F, Watson, C, da Silva, EA, Muzik, O, Chugani, DC, Shah, J, Chugani, HT., 1999. Glucose and [11C]flumazenil positron emission tomography abnormalities of thalamic nuclei in temporal lobe epilepsy. Neurology 53 (9), 2037–2045. doi:10.1212/wnl.53.9.2037, PMID: 10599778.

Keating, GL, Kuhar, MJ, Rye, DB, 2008. High dose CART peptide induces abnormal EEG activity and behavioral seizures. Neuropeptides 42 (2), 199–204. doi:10.1016/j.npep.2007.11.005.

Klingler, J, Gloor, P., 1960. The connections of the amygdala and of the anterior temporal cortex in the human brain. J. Comp. Neurol. 115, 333–369. doi:10.1002/cne.901150305, PMID: 13756891.

Kochanski, RB., Dawe, R, Eddelman, DB, Kocak, M, Sani, S., 2016. Identification of the stria medullaris thalami using diffusion tensor imaging. Neuroimage Clin. 12, 852–857. doi:10.1016/j.nicl.2016.10.018.

Koeppen, JA, Nahravani, F, Kramer, M, Voges, B, House, PM, Gulberti, A, Moll, CKE, Westphal, M, Hamel, W., 2019. Electrical stimulation of the anterior thalamus for epilepsy: clinical outcome and analysis of efficient target. Neuromodulation 22 (4), 465–471. doi:10.1111/ner.12865, Epub 2018 Oct 8. PMID: 30295358.

Kreilkamp, BAK, McKavanagh, A, Alonazi, B, Bryant, L, Das, K, Wieshmann, UC, Marson, AG, Taylor, PN, Keller, SS., 2021. Altered structural connectome in non-lesional newly diagnosed focal epilepsy: relation to pharmacoresistance. Neuroimage Clin. 29, 102564. doi:10.1016/j.nicl.2021.102564, Epub 2021 Jan 19. PMID: 33508622; PMCID: PMC7841400.

Kremer, S, Braun, M, Kahane, P, Guillemin, F, Le Bas, JF, Benabid, AL, 2003. MRI morphological and volumetric study of the cingulate gyrus and its relevance in partial epileptic patients. Epileptic Disord. J. Videotape 5 (2), 101–107 PMID: 12875953.

Krieg, WJS, 1973. Architectonics of Human Cerebral Fiber Systems. Brain Books, Evanston.

Krishna, V, King, NK, Sammartino, F, Strauss, I, Andrade, DM, Wennberg, RA, Lozano, AM., 2016. Anterior nucleus deep brain stimulation for refractory epilepsy: insights into patterns of seizure control and efficacious target. Neurosurgery 78 (6), 802–811. doi:10.1227/NEU.0000000000001197.

Kuhlenbeck, H, 1951. The derivatives of thalamus dorsalis and epithalamus in the human brain: their relation to cortical and other centers. Military Surgeon 108 (3), 205–256 PMID: 14806148.

Lawes, IN, Barrick, TR, Murugam, V, Spierings, N, Evans, DR, Song, M, Clark, CA., 2008. Atlas-based segmentation of white matter tracts of the human brain using diffusion tensor tractography and comparison with classical dissection. Neuroimage 39 (1), 62–79. doi:10.1016/j.neuroimage.2007.06.041, Epub 2007 Aug 7. PMID: 17919935.

Lehtimäki, K, Möttönen, T, Järventausta, K, Katisko, J, Tähtinen, T, Haapasalo, J, Niskakangas, T, Kiekara, T, Öhman, J, Peltola, J., 2016. Outcome based definition of the anterior thalamic deep brain stimulation target in refractory epilepsy. Brain Stimul. 9 (2), 268–275. doi:10.1016/j.brs.2015.09.014, Epub 2015 Oct 9. PMID: 26680105.

Letinic, K, Rakic, P., 2001. Telencephalic origin of human thalamic GABAergic neurons. Nat. Neurosci. 4 (9), 931–936. doi:10.1038/nn0901-931, PMID: 11528425.

Liao, W, Zhang, Z, Pan, Z, Mantini, D, Ding, J, Duan, X, Luo, C, Lu, G, Chen, H., 2010. Altered functional connectivity and small-world in mesial temporal lobe epilepsy. PLoS One 5 (1), e8525. doi:10.1371/journal.pone.0008525, PMID: 20072616; PMCID: PMC2799523.

Lindvall, O, Björklund, A, 1983. Dopamine- and norepinephrine-containing neuron systems: their anatomy in the rat brain. In: Emson, P.C. (Ed.), Chemical Neuroanatomy. Raven Press, New York, pp. 229–256.

Lujan, JL, Chaturvedi, A, Choi, KS, Holtzheimer, PE, Gross, RE, Mayberg, HS, McIntyre, CC., 2013. Tractography-activation models applied to subcallosal cingulate deep brain stimulation. Brain Stimul. 6 (5), 737–739. doi:10.1016/j.brs.2013.03.008, Epub 2013 Apr 6. PMID: 23602025; PMCID: PMC3772993.

Mai, JK, Forutan, F., 2012. Thalamus. In: Mai, J.K., Paxinos, G. (Eds.), The Human Nervous System. Academic Press/Elsevier, San Diego, pp. 620–679.

Mai, JK, Majtanik, M, Paxinos, G., 2015. Atlas of the Human Brain, 4th Ed. Academic Press, San Diego ISBN: 9780128028001.

Mai, JK, Majtanik, M., 2010. MRX Atlas of the Human Brain (unpublished), representing the left hemisphere of the “Atlas of the Human Brain. Academic Press, San Diego additionally integrating information from histological and histochemical sections of other brains from the Dept. of Anatomy I, Duesseldorf.

Mai, JK, Majtanik, M, 2017. *Human Brain in Standard MNI Space: A Comprehensive Pocket Atlas*. Academic Press/Elsevier, San Diego, CA.

Mai, JK, Majtanik, M., 2019. Toward a common terminology for the Thalamus. Front. Neuroanat. 12, 114. doi:10.3389/fnana.2018.00114, PMID: 30687023; PMCID: PMC6336698.

Maier-Hein, KH, Neher, PF, Houde, JC, Côté, MA, Garyfallidis, E, Zhong, J, Chamberland, M, Yeh, FC, Lin, YC, Ji, Q, Reddick, WE, Glass, JO, Chen, DQ, Feng, Y, Gao, C, Wu, Y, Ma, J, He, R, Li, Q, Westin, CF, Deslauriers-Gauthier, S, González, JOO, Paquette, M, St-Jean, S, Girard, G, Rheault, F, Sidhu, J, Tax, CMW, Guo, F, Mesri, HY, Dávid, S, Froeling, M, Heemskerk, AM, Leemans, A, Boré, A, Pinsard, B, Bedetti, C, Desrosiers, M, Brambati, S, Doyon, J, Sarica, A, Vasta, R, Cerasa, A, Quattrone, A, Yeatman, J, Khan, AR, Hodges, W, Alexander, S, Romascano, D, Barakovic, M, Auría, A, Esteban, O, Lemkaddem, A, Thiran, JP, Cetingul, HE, Odry, BL, Mailhe, B, Nadar, MS, Pizzagalli, F, Prasad, G, Villalon-Reina, JE, Galvis, J, Thompson, PM, Requejo, FS, Laguna, PL, Lacerda, LM, Barrett, R, Dell'Acqua, F, Catani, M, Petit, L, Caruyer, E, Daducci, A, Dyrby, TB, Holland-Letz, T, Hilgetag, CC, Stieltjes, B, Descoteaux, M, 2017. The challenge of mapping the human connectome based on diffusion tractography. Nat. Commun. 8 (1), 1349. doi:10.1038/s41467-017-01285-x, Erratum in: Nat Commun. 2019 Nov 4;10(1):5059. PMID: 29116093; PMCID: PMC5677006.

Majtanik, M, Mai, JK, Gielen, FLH, Lehtimäki, K, Coenen, VA, Gil-Nagel, A, Gonçalves Ferreira, AJ, Peltola, JT, Ryvlin, P, Abouihia, A, Brionne, TC, 2021. Towards Refined Targeting the Anterior Nucleus of Thalamus in DBS for Epilepsy. ESSFN, Marseille Sept 2021.

Mathiasen, ML, O'Mara, SM, Aggleton, JP, 2020. The anterior thalamic nuclei and nucleus reuniens: so similar but so different. Neurosci. Biobehav. Rev. 119, 268–280. doi:10.1016/j.neubiorev.2020.10.006, Google Scholar.

Matsuoka, H., 1986. Topographic arrangement of the projection from the anterior thalamic nuclei to the cingulate cortex in the cat. Neurosci. Res. 4 (1), 62–66. doi:10.1016/0168-0102(86)90017-9, PMID: 3808482.

Meys, KME, de Vries, LS, Groenendaal, F, Vann, SD, Lequin, MH., 2022. The mammillary bodies: a review of causes of injury in infants and children. AJNR Am. J. Neuroradiol. doi:10.3174/ajnr.A7463, Epub ahead of print. PMID: 35487586.

Middlebrooks, EH, Grewal, SS, Stead, M, Lundstrom, BN, Worrell, GA, Van Gompel, JJ., 2018. Differences in functional connectivity profiles as a predictor of response to anterior thalamic nucleus deep brain stimulation for epilepsy: a hypothesis for the mechanism of action and a potential biomarker for outcomes. Neurosurg. Focus 45 (2), E7. doi:10.3171/2018.5.FOCUS18151, AugPMID: 30064322.

Middlebrooks, EH, Ver Hoef, L, Szaflarski, JP, 2017. Neuroimaging in Epilepsy. Curr. Neurol. Neurosci. Rep. 17 (4), 32. doi:10.1007/s11910-017-0746-x, PMID: 28324301.

Miller, JW, Turner, GM, Gray, BC., 1994. Anticonvulsant effects of the experimental induction of hippocampal theta activity. Epilepsy Res. 18, 195–204. doi:10.1016/0920-1211(94)90040-X.

Mufson, EJ, Pandya, DN., 1984. Some observations on the course and composition of the cingulum bundle in the rhesus monkey. J. Comp. Neurol. 225 (1), 31–43. doi:10.1002/cne.902250105, PMID: 6725639.

Nauta, WJH, 1962. Neural associations of the amygdaloid complex in the monkey. Brain 85, 505–520. doi:10.1093/brain/85.3.505, PMID: 13937752.

Nauta, WJH., Haymaker, W., 1969. Hypothalamic nuclei and fiber connections. In: The Hypothalamus. Charles C. Thomas, Springfield IL, pp. 136–209.

Ng, MC., 2017. Orexin and Epilepsy: Potential Role of REM Sleep. Sleep 40 (3), zsw061. doi:10.1093/sleep/zsw061, 1 March 2017.

Nieuwenhuys, R, Geeraedts, LM, Veening, JG., 1982. The medial forebrain bundle of the rat. I. General introduction. J. Comp. Neurol. 206 (1), 49–81. doi:10.1002/cne.902060106, PMID: 6124562.

Ongür, D, Price, JL., 2000. The organization of networks within the orbital and medial prefrontal cortex of rats, monkeys and humans. Cereb. Cortex 10, 206–219. doi:10.1093/cercor/10.3.206.

Osorio, I, Giftakis, J, Stypulkowski, P, Tonder, L., 2021. Anatomical connectivity and efficacy of electro-therapy for seizure control: a SANTE's single-center regression analyses. Epilepsy Behav. 115, 107709. doi:10.1016/j.yebeh.2020.107709.

Pabba, M., 2013. Evolutionary development of the amygdaloid complex. Front. Neuroanat. 7, 27. doi:10.3389/fnana.2013.00027, PMID: 24009561; PMCID: PMC3755265.

Patel, DC, Tewari, BP, SontheimerH, Chaunsali L., 2019. Neuron–glia interactions in the pathophysiology of epilepsy. Nat. Rev. Neurosci. 20, 282–297. doi:10.1038/s41583-019-0126-4.

Percheron, G., 2004. Thalamus. In: Paxinus, G., Mai, J.K. (Eds.), The Human Nervous System. Elsevier, Academic Press, San Diego, pp. 439–468.

Pereira, FR, Alessio, A, Sercheli, MS, Pedro, T, Bilevicius, E, Rondina, JM, Ozelo, HF, Castellano, G, Covolan, RJ, Damasceno, BP, Cendes, F., 2010. Asymmetrical hippocampal connectivity in mesial temporal lobe epilepsy: evidence from resting state fMRI. BMC Neurosci. 11, 66. doi:10.1186/1471-2202-11-66, PMID: 20525202; PMCID: PMC2890013.

Poletti, C, Creswell, G, 1977. Fornix system efferent projections in the squirrel monkey: an experimental degeneration study. J. Comp. Neurol. 175, 101–127. doi:10.1002/cne.901750107.

Post, S, Mai, JK., 1980. Contribution to the amygdaloid projection field in the rat. A quantitative autoradiographic study. J. Hirnforsch. 21, 199–225 PMID: 6967499.

Proix, T, Jirsa, VK, Bartolomei, F, Guye, M, Truccolo, W., 2018. Predicting the spatiotemporal diversity of seizure propagation and termination in human focal epilepsy. Nat. Commun. 9, 1088. doi:10.1038/s41467-018-02973-y.

Riley, HA., 1960. An Atlas of the Basal Ganglia, Brain Stem and Spinal Cord. Hafner, New York.

Robertson, RT, Kaitz, SS., 1981. Thalamic connections with limbic cortex. I. Thalamocortical projections. J. Comp. Neurol. 195 (3), 501–525. doi:10.1002/cne.901950308.

Roddy, DW, Roman, E, Rooney, S, Andrews, S, Farrell, C, Doolin, K, Levins, KJ, Tozzi, L, Tierney, P, Barry, D, Frodl, T, O'Keane, V, O'Hanlon, E., 2018. Awakening neuropsychiatric research into the stria medullaris: development of a diffusion-weighted imaging tractography protocol of this key limbic structure. Front. Neuroanatomy 12, 39. doi:10.3389/fnana.2018.00039.

Saalmann, YB., 2004. Intralaminar and medial thalamic influence on cortical synchrony, information transmission and cognition. Front. Syst. Neurosci. doi:10.3389/fnsys.2014.00083, 09 May 2014.

Sachs, E., 1909. On the structure and functional relations of the optic thalamus. Brain 32 (2), 95–186. doi:10.1093/brain/32.2.95.

Safadi, Z, Grisot, G, Jbabdi, S, Behrens, TE, Heilbronner, SR, McLaughlin, NCR, Mandeville, J, Versace, A, Phillips, ML, Lehman, JF, Yendiki, A, Haber, SN., 2018. Functional segmentation of the anterior limb of the internal capsule: linking white matter abnormalities to specific connections. J. Neurosci. 38 (8), 2106–2117. doi:10.1523/JNEUROSCI.2335-17.2017, Epub 2018 Jan 22. PMID: 29358360; PMCID: PMC5824744.

Salanova, V, Witt, T, Worth, R, Henry, TR, Gross, RE, Nazzaro, JM, Labar, D, Sperling, MR, Sharan, A, Sandok, E, Handforth, A, Stern, JM, Chung, S, Henderson, JM, French, J, Baltuch, G, Rosenfeld, WE, Garcia, P, Barbaro, NM, Fountain, NB, Elias, WJ, Goodman, RR, Pollard, JR, Tröster, AI, Irwin, CP, Lambrecht, K, Graves, N, Fisher, R, 2015. Long-term efficacy and safety of thalamic stimulation for drug-resistant partial epilepsy. Neurology 84 (10), 1017–1025. doi:10.1212/WNL.0000000000001334, 2015 Mar 10Epub 2015 Feb 6. PMID: 25663221; PMCID: PMC4352097.

Samadani, U, Baltuch, GH., 2007. Anterior thalamic nucleus stimulation for epilepsy. Acta Neurochir. 97 (Pt 2), 343–346. doi:10.1007/978-3-211-33081-4_39, SupplPMID: 17691322.

Schaper, FLWVJ, Plantinga, BR, Colon, AJ, Wagner, GL, Boon, P, Blom, N, Gommer, EG, Hoogland, G, Ackermans, A, Rouhl, BPW, Temel, Y, 2020. Deep brain stimulation in epilepsy: a role for modulation of the mammillothalamic tract in seizure control? Neurosurgery 87 (3), 602–610. doi:10.1093/neuros/nyaa141, PMID: 32421806; PMCID: PMC8210468.

Schilling, KG, Nath, V, Hansen, C, Parvathaneni, P, Blaber, J, Gao, Y, Neher, P, Aydogan, DB, Shi, Y, Ocampo-Pineda, M, Schiavi, S, Daducci, A, Girard, G, Barakovic, M, Rafael-Patino, J, Romascano, D, Rensonnet, G, Pizzolato, M, Bates, A, Fischi, E, Thiran, JP, Canales-Rodríguez, EJ, Huang, C, Zhu, H, Zhong, L, Cabeen, R, Toga, AW, Rheault, F, Theaud, G, Houde, JC, Sidhu, J, Chamberland, M, Westin, CF, Dyrby, TB, Verma, R, Rathi, Y, Irfanoglu, MO, Thomas, C, Pierpaoli, C, Descoteaux, M, Anderson, AW, Landman, BA., 2019. Limits to anatomical accuracy of diffusion tractography using modern approaches. Neuroimage 185, 1–11. doi:10.1016/j.neuroimage.2018.10.029, Epub 2018 Oct 11. PMID: 30317017; PMCID: PMC6551229.

Schilling, KG, Rheault, F, Petit, L, Hansen, CB, Nath, V, Yeh, FC, Girard, G, Barakovic, M, Rafael-Patino, J, Yu, T, Fischi-Gomez, E, Pizzolato, M, Ocampo-Pineda, M, Schiavi, S, Canales-Rodríguez, EJ, Daducci, A, Granziera, C, Innocenti, G, Thiran, JP, Mancini, L, Wastling, S, Cocozza, S, Petracca, M, Pontillo, G, Mancini, M, Vos, SB, Vakharia, VN, Duncan, JS, Melero, H, Manzanedo, L, Sanz-Morales, E, Á, Peña-Melián, Calamante, F, Attyé, A, Cabeen, RP, Korobova, L, Toga, AW, Vijayakumari, AA, Parker, D, Verma, R, Radwan, A, Sunaert, S, Emsell, L, De Luca, A, Leemans, A, Bajada, CJ, Haroon, H, Azadbakht, H, Chamberland, M, Genc, S, Tax, CMW, Yeh, PH, Srikanchana, R, Mcknight, CD, Yang, JY, Chen, J, Kelly, CE, Yeh, CH, Cochereau, J, Maller, JJ, Welton, T, Almairac, F, Seunarine, KK, Clark, CA, Zhang, F, Makris, N, Golby, A, Rathi, Y, O'Donnell, LJ, Xia, Y, Aydogan, DB, Shi, Y, Fernandes, FG, Raemaekers, M, Warrington, S, Michielse, S, Ramírez-Manzanares, A, Concha, L, Aranda, R, Meraz, MR, Lerma-Usabiaga, G, Roitman, L, Fekonja, LS, Calarco, N, Joseph, M, Nakua, H, Voineskos, AN, Karan, P, Grenier, G, Legarreta, JH, Adluru, N, Nair, VA, Prabhakaran, V, Alexander, AL, Kamagata, K, Saito, Y, Uchida, W, Andica, C, Abe, M, Bayrak, RG, Wheeler-Kingshott, CAMG, D'Angelo, E, Palesi, F, Savini, G, Rolandi, N, Guevara, P, Houenou, J, López-López, N, Mangin, JF, Poupon, C, Román, C, Vázquez, A, Maffei, C, Arantes, M, Andrade, JP, Silva, SM, Calhoun, VD, Caverzasi, E, Sacco, S, Lauricella, M, Pestilli, F, Bullock, D, Zhan, Y, Brignoni-Perez, E, Lebel, C, Reynolds, JE, Nestrasil, I, Labounek, R, Lenglet, C, Paulson, A, Aulicka, S, Heilbronner, SR, Heuer, K, Chandio, BQ, Guaje, J, Tang, W, Garyfallidis, E, Raja, R, Anderson, AW, Landman, BA, Descoteaux, M., 2021. Tractography dissection variability: what happens when 42 groups dissect 14 white matter bundles on the same dataset? Neuroimage 243, 118502. doi:10.1016/j.neuroimage.2021.118502, Epub 2021 Aug 22. PMID: 34433094.

Schmahmann, JD, Pandya, DN, Wang, R, Dai, G, D'Arceuil, HE, de Crespigny, AJ, Wedeen, VJ., 2007. Association fibre pathways of the brain: parallel observations from diffusion spectrum imaging and autoradiography. Brain 130 (Pt 3), 630–653. doi:10.1093/brain/awl359, Epub 2007 Feb 9. PMID: 17293361.

Schmidt, D, Löscher, W., 2005. Drug resistance in epilepsy: putative neurobiologic and clinical mechanisms. Epilepsia 46 (6), 858–877. doi:10.1111/j.1528-1167.2005.54904.x, PMID: 15946327.

Seki, M, Zyo, K., 1984. Anterior thalamic afferents from the mamillary body and the limbic cortex in the rat. J. Comp. Neurol. 229, 242–256. doi:10.1002/cne.902290209, PMID: 6438191.

Shibata, H, 1984. Anterior thalamic afferents from the mamillary body and the limbic cortex in the rat. J. Comp. Neurol. 323 (1), 117–127. doi:10.1002/cne.903230110, PMID: 1385491.

Shibata, H., Yukie, M., 1990. Thalamocingulate connections in the monkey. In: Vogt, B.A. (Ed.), Cingulate Neurobiology and Disease. Oxford University Press, Oxford, pp. 95–111.

Sikes, RW, Chronister, RB, White, LE., 1977. Origin of the direct hippocampus-anterior thalamic bundle in the rat: A combined horseradish peroxidase-Golgi analysis. Exp. Neurol. 57, 379–395.

Smith, R.E., Tournier, J.-D., Calamante, F., Connelly, A., 2012. Anatomically-constrained tractography: Improved diffusion MRI streamlines tractography through effective use of anatomical information. Neuroimage 62, 1924–1938.

Smith, RE, Tournier, JD, Calamante, F, Connelly, A., 2015. SIFT2: enabling dense quantitative assessment of brain white matter connectivity using streamlines tractography. Neuroimage 119, 338–351. doi:10.1016/j.neuroimage.2015.06.092, 1.

Sorokin, JM, Davidson, TJ, Frechette, E, Abramian, AM, Deisseroth, K, Huguenard, JR, Paz, JT., 2017. Bidirectional control of generalized epilepsy networks via rapid real-time switching of firing mode. Neuron 93 (1), 194–210. doi:10.1016/j.neuron.2016.11.026, Epub 2016 Dec 15. PMID: 27989462; PMCID: PMC5268077.

Stypulkowski, PH, Stanslaski, SR, Jensen, RM, Denison, TJ, Giftakis, JE., 2014. Brain stimulation for epilepsy—local and remote modulation of network excitability. Brain Stimul. 7, 350–358. doi:10.1016/j.brs.2014.02.002.

Sutherland, FJ., 1982. The dorsal diencephalic conduction system: a review of the anatomy and functions of the habenular complex. Neurosci. Biobehav. Rev. 6 (1), 1–13. doi:10.1016/0149-7634(82)90003-3, PMID: 7041014.

Swanson, LW, Cowan, WM., 1977. An autoradiographic study of the organization of the efferet connections of the hippocampal formation in the rat. J. Comp. Neurol. 172 (1), 49–84. doi:10.1002/cne.901720104, PMID: 65364.

Thomas, C, Ye, FQ, Irfanoglu, MO, Modi, P, Saleem, KS, Leopold, DA, Pierpaoli, C., 2014. Anatomical accuracy of brain connections derived from diffusion MRI tractography is inherently limited. Proc. Natl. Acad. Sci. U S A. 111 (46), 16574–16579. doi:10.1073/pnas.1405672111, Epub 2014 Nov 3. PMID: 25368179; PMCID: PMC4246325.

Tomitaka, S, Tomitaka, M, Tolliver, BK, Sharp, FR., 2000. Bilateral blockade of NMDA receptors in anterior thalamus by dizocilpine (MK-801) injures pyramidal neurons in rat retrosplenial cortex. Eur. J. Neurosci. 12 (4), 1420–1430. doi:10.1046/j.1460-9568.2000.00018.x, AprPMID: 10762370.

Tournier, J.D., Smith, R., Raffelt, D., Tabbara, R., Dhollander, T., Pietsch, M., Christiaens, D., Jeurissen, B., Yeh, C.H., Connelly, A., 2019. MRtrix3: A fast, flexible and open software framework for medical image processing and visualisation. Neuroimage 202, 116137. doi:10.1016/j.neuroimage.2019.116137.

Tournier, J.-D., Calamante, F., Connelly, A., 2012. MRtrix: diffusion tractography in crossing fiber regions. Int. J. Imag. Syst. Technol. 22 (1), 53–66.

Tournier, JD, Calamante, F, Connelly, A., 2007. Robust determination of the fibre orientation distribution in diffusion MRI: non-negativity constrained super-resolved spherical deconvolution. Neuroimage 35 (4), 1459–1472. doi:10.1016/j.neuroimage.2007.02.016, Epub 2007 Feb 21. PMID: 17379540.

Tournier, JD, Calamante, F, Gadian, DG, Connelly, A., 2004. Direct estimation of the fiber orientation density function from diffusion-weighted MRI data using spherical deconvolution. Neuroimage 23 (3), 1176–1185. doi:10.1016/j.neuroimage.2004.07.037, PMID: 15528117.

Van Essen, DC, Smith, SM, Barch, DM, Behrens, TE, Yacoub, E, Ugurbil, K, 2013. The WU-Minn human connectome project: an overview. Neuroimage 80, 62–79. doi:10.1016/j.neuroimage.2013.05.041, Epub 2013 May 16. PMID: 23684880; PMCID: PMC3724347.

Velísková, J, Moshé, SL., 2006. Update on the role of substantia nigra pars reticulata in the regulation of seizures. Epilepsy Curr. 6 (3), 83–87. doi:10.1111/j.1535-7511.2006.00106.x, PMID: 16761069; PMCID: PMC1464157.

Vismer, MS, Forcelli, PA, Skopin, MD, Gale, K, Koubeissi, MZ., 2015. The piriform, perirhinal, and entorhinal cortex in seizure generation. Front. Neural Circuits 9, 27. doi:10.3389/fncir.2015.00027.

Voges, BR, Schmitt, FC, Hamel, W, House, PM, Kluge, C, Moll, CK, Stodieck, SR., 2015. Deep brain stimulation of anterior nucleus thalami disrupts sleep in epilepsy patients. Epilepsia 56 (8), e99–e103. doi:10.1111/epi.13045, Epub 2015 Jun 4. PMID: 26041007.

Vogt, BA, Pandya, DN, Rosene, DL, 1987. Cingulate cortex of the rhesus monkey: I. Cytoarchitecture and thalamic afferents. J. Comp. Neurol. 262 (2), 256–270. doi:10.1002/cne.902620207, PMID: 3624554.

Vogt, BA., 2009. Regions and subregions of the cingulate cortex. Brent A Vogt: Cingulate Neurobiology and Disease. OUP, Oxford, GB.

Vogt, C, Vogt, O., 1904. Die Markreifung des Kindergehirns während der ersten vier Lebensmonate und ihre methodologische Bedeutung. Neurobiologische Arbeiten. Beiträge zur Hirnfaserlehre. G. Fischer, Jena Vol. 1Fig. 150.

Vonck, K, Boon, P, Van Roost, D., 2007. Anatomical and physiological basis and mechanism of action of neurostimulation for epilepsy. Acta Neurochir. Suppl. 97, 321–328. doi:10.1007/978-3-211-33081-4_35.

Waller, WH., 1933. Topographical relations of cortical lesions to thalamic nuclei in the albino rat. J. Comp. Neurol. 60 (2), 237–269. doi:10.1002/cne.900600205.

Walter, A, Mai, JK, Lanta, L, Görcs, T., 1991. Differential distribution of immunohistochemical markers in the bed nucleus of the stria terminalis in the human brain. J. Chem. Neuroanat. 4 (4), 281–298. doi:10.1016/0891-0618(91)90019-9, PMID: 1718318.

Wang, Y, Tan, B, Wang, Y, Chen, Z, 2021. Cholinergic Signaling, Neural Excitability, and Epilepsy. Molecules 26 (8), 2258. doi:10.3390/molecules26082258, PMID: 33924731; PMCID: PMC8070422.

Weininger, J, Roman, E, Tierney, P, Barry, D, Gallagher, H, Murphy, P, Levins, KJ, O'Keane, V, O'Hanlon, E, Roddy, DW, 2019. Papez's forgotten tract: 80 years of unreconciled findings concerning the thalamocingulate tract. Front. Neuroanat. 13, 14. doi:10.3389/fnana.2019.00014, Feb 18.

Whitlock, DG, Naut, WJH., 1956. Subcortical projections from the temporal neocortex in Macaca mulatta. J. Comp. Neurol. 106 (1), 183–212. doi:10.1002/cne.901060107, PMID: 13398494.

Wicker, E, Beck, VC, Kulick-Soper, C, Kulick-Soper, CV, Hyder, SK, Campos-Rodriguez, C, Khan, T, N'Gouemo, P, Forcelli, PA, 2019. Descending projections from the substantia nigra pars reticulata differentially control seizures. Proc. Natl. Acad. Sci. U S A. 116 (52), 27084–27094. doi:10.1073/pnas.1908176117, Epub ahead of print. PMID: 31843937; PMCID: PMC6936676.

Wirsich, J, Perry, A, Ridley, B, Proix.T, Golos M, Bénar, C, J-Ph, Ranjeva, Bartolomei, F, Breakspear, M, Jirsa, V, Guye, M, 2016. Whole-brain analytic measures of network communication reveal increased structurefunction correlation in right temporal lobe epilepsy. Neuroimage Clin. 11, 707–718. doi:10.1016/j.nicl.2016.05.010.

Yakovlev, PI, Locke, DY, Koskoff, DY, Patton, RA., 1960. Limbic nuclei of thalamus and connectons of limbic cortex. I. Organization of the projections of the anterior group

of nuclei and of the midline nuclei of the thalamus to the anterior cingulate gyrus and hippocampal rudiment in the monkey. Arch. Neurol. 3, 620–641. doi:10.1001/archneur.1960.00450060008002, PMID: 13787071.

Yakovlev, PI, Locke, DY., 1961. Limbic nuclei of thalamus and connections of limbic cortex. III. Corticocortical connections of the anterior cingulate gyrus, the cingulum, and the subcallosal bundle in monkey. Arch. Neurol. 5, 364–400. doi:10.1001/archneur.1961.00450160014002, PMID: 14008719.

Zangiabadi, N, Ladino, LD, Sina, F, Orozco-Hernández, JP, Carter, A, Téllez-Zenteno, JF., 2019. Deep brain stimulation and drug-resistant epilepsy: a review of the literature. Front. Neurol. 10, 601. doi:10.3389/fneur.2019.00601.

Zhan, Q, Buchanan, GF, Motelow, JE, Andrews, J, Vitkovskiy, P, Chen, WC, Serout, F, Gummadavelli, A, Kundishora, A, Furman, M, Li, W, Bo, X, Richerson, GB, Blumenfeld, H., 2016. Impaired serotonergic brainstem function during and after seizures. J. Neurosci. 36 (9), 2711–2722. doi:10.1523/JNEUROSCI.4331-15.2016, PMID: 26937010; PMCID: PMC4879214.

Zumsteg, D, Lozano, AM, Wieser, HG, Wennberg, 2006. Cortical activation with deep brain stimulation of the anterior thalamus for epilepsy. Clin. Neurophysiol. 117 (1), 192–207. doi:10.1016/j.clinph.2005.09.015, Jan.

Zyo, K, Oki, T, Ban, T., 1963. Experimental studies on the medial forebrain bundle, medial longitudinal fasciculus and supraoptic decussations in the rabbit. Med. J. Osaka Univ. 13, 193–239 PMID: 14004175.

Further Reading

Costa-Gertrudes, R, Simão, D, Franco, A, Morgado, C, Peralta, A, R, Pimentel, J, Gonçalves-Ferreira, A, Bentes, C, Campos A, R., 2022. Anterior nucleus of thalamus deep brain stimulation: a clinical-based analysis of the ideal target in drug-resistant epilepsy. Stereotact. Funct. Neurosurg. 100, 108–120. doi:10.1159/000519917.